EURASIP Journal on Applied Signal Processing 2005:3, 328–345

Performance Analysis and Comparison of Time-Hopping and Direct-Sequence UWB-MIMO Systems

W. Pam Siriwongpairat
Department of Electrical and Computer Engineering, University of Maryland, College Park, MD 20742, USA
Email: wipawee@eng.umd.edu

Masoud Olfat
Department of Electrical and Computer Engineering, University of Maryland, College Park, MD 20742, USA
Email: molfat@eng.umd.edu

K. J. Ray Liu
Department of Electrical and Computer Engineering, University of Maryland, College Park, MD 20742, USA
Email: kjrliu@eng.umd.edu

Received 15 October 2003; Revised 5 April 2004

We analyze the performance of ultra-wideband (UWB) multiple-input multiple-output (MIMO) systems employing various modulation and multiple access (MA) schemes including time-hopping (TH) binary pulse-position modulation (BPPM), TH binary phase-shift keying (BPSK), and direct-sequence (DS-) BPSK. We quantify the performance merits of UWB space-time (ST) systems regardless of specific coding scheme. For each modulation technique, we introduce a framework that enables us to compare UWB-MIMO systems with conventional UWB single-input single-output (SISO) systems in terms of diversity and coding gains. We show that the combination of ST coding and RAKE receiver is capable of exploiting spatial diversity as well as multipath diversity, richly inherent in UWB environments. In addition, we adopt the real orthogonal design (ROD) as the engine code for UWB-ST codes. We find the upper bound of the average pairwise error probability (PEP) under the hypothesis of quasistatic Nakagami-m frequency-selective fading channels. The performance comparison of ROD-ST codes with different rates is also addressed. Finally, simulation results are presented to support the theoretical analysis.

Keywords and phrases: ultra-wideband, time hopping, direct sequence, UWB-MIMO, multiple antennas, space-time coding.

1. INTRODUCTION

Ultra-wideband (UWB) technology has recently gained considerable interest due to the Federal Communications Commission (FCC) approval, which allows the use of UWB on an unlicensed basis following the Part 15 rules [1]. UWB transmission, also referred to as impulse communications, is characterized by a sequence of extremely short duration, broad spectrum chirps of radio waves. According to the FCC definition, UWB technology is a transmission scheme that occupies a bandwidth of more than 20% of its center frequency, or nominally more than 500 MHz. The UWB nature offers several advantages over narrowband technology including high data rate, extensive multipath diversity, low power consumption, and support for multiple access (MA) [2]. These unique characteristics of UWB make it a viable candidate for future short-range wireless communications, especially indoor wireless and home entertainment systems. However, since UWB utilizes overlapping frequencies with the existing narrowband devices, its transmit power spectral density is limited according to the FCC regulations [1]. For example, the FCC Part 15.209 rules limit the emissions for intentional radiators to 500 μV/m (measured at 3 m distance in a 1 MHz bandwidth) for a frequency range of 3.1–10.6 GHz. This corresponds to a transmitted power spectral density of -41.3 dBm/MHz. Such constraint is one of the technical challenges in designing UWB systems. In order to achieve the expected performance with the limited power, various aspects of UWB system designs have been studied. One consideration is to make use of numerous propagation paths available in dense multipath indoor environments [3].

Space-time (ST) coded multiple-input multiple-output (MIMO) system has been well known for its effectiveness

in improving system performance under multipath scenarios. A key concept to approach such improvement is through ST coding (see e.g., [4, 5, 6]), which is based on introducing joint processing in time, the natural dimension of communication data, as well as in space via the use of multiple spatially distributed antennas. Through this approach, MIMO can provide both diversity and coding gains, simultaneously, and hence yield high spectral efficiency and remarkable quality improvement.

To exploit the advantages of both UWB and MIMO systems, UWB-MIMO systems have been proposed [7, 8, 9, 10]. The authors in [7] suggested an UWB-ST-coded system based on the repetition code, which is a special case of what we present in this work. In this paper, we consider UWB-ST systems with various modulation and MA schemes, including time-hopping (TH) binary pulse-position modulation (BPPM) [11], TH binary phase-shift keying (BPSK) [12], and direct-sequence (DS-) BPSK [13, 14]. In the TH-based system, the information is sent with a time offset for each pulse determined by a TH sequence, whereas for the DS spreading system, the data is carried in multiple pulses whose amplitudes are based upon a certain spreading code. Both TH and DS spreading codes provide robustness against multiuser interference. The performance comparisons of TH and DS schemes for single-antenna systems have been studied in [15, 16]. It has been shown that TH-UWB systems are suitable in theory and analysis but are little, if ever, used in practice (e.g., see the IEEE 802.15.3a standards process at http://www.ieee802.org/15/pub/TG3a.html). On the other hand, DS-UWB has been shown to be a promising scheme for single-carrier UWB communications. Recently, the two leading proposals for IEEE 802.15.3a wireless personal area networking (WPAN) standard are based on DS-UWB and multiband orthogonal frequency division multiplexing (MB-OFDM) approaches (see UWB Multiband Coalition at http://www.uwbmultiband.org). MB-OFDM divides the UWB spectrum into multiple bands and utilizes multicarrier transmission. It combats the detrimental effects of multipath fading by the use of OFDM.

In this paper, we consider various single-carrier UWB-MIMO modulation schemes. We quantify the performance figures of TH- and DS-UWB-MIMO systems regardless of specific coding schemes. We adopt the stochastic tapped delay line (STDL) channel model [17] which enables us to take into consideration the frequency selectivity of UWB channels. For both TH and DS schemes, we devise a theoretical framework to characterize the performances of UWB-ST systems with the diversity and the coding advantages. Even though the antenna characteristics do not remain constant over the large bandwidth of UWB systems, by applying the second derivative of Gaussian pulses at the receiver, we can equalize the variations of antenna characteristics due to large frequency bandwidth [18, 19]. We also utilize the real orthogonal design (ROD) [6] as the engine code for UWB-ST codes. Our simulation results show the performance improvement of UWB-MIMO systems over the conventional single-input single-output (SISO) systems for every modulation and MA technique. Furthermore, we show that DS-UWB-MIMO transmission provides superior performance in both single-user and multiuser scenarios.

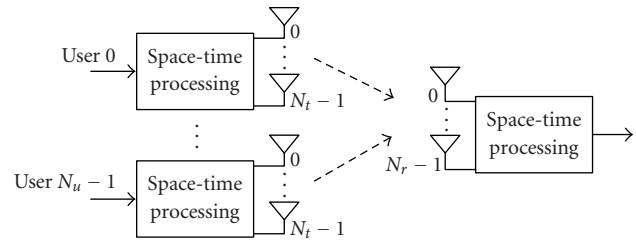

Figure 1: UWB-MIMO multiuser system.

The rest of the paper is organized as follows. Section 2 describes the models of UWB-ST signals utilizing TH-BPPM, TH-BPSK, and DS-BPSK schemes. The structure of UWB-MIMO receivers and the analysis of the received UWB-ST signals are presented in Section 3. In Section 4, we investigate the system performances in terms of the upper bound of the pairwise error probability (PEP). The performances of UWB-ROD-ST codes with different rates are evaluated in Section 5. Section 6 describes numerical results, and finally Section 7 concludes the paper.

2. UWB-ST SIGNAL MODELS

We consider UWB-MIMO multiuser environment with N_u users, each equipped with N_t transmit antennas, and a receiver with N_r receive antennas as shown in Figure 1. For each user, the input binary symbol sequence (coded or uncoded) is divided into blocks of N_b symbols. Each block is encoded into an ST codeword to be transmitted over N_t transmit antennas during K time slots. The ST codeword matrix can be expressed as an $K \times N_t$ matrix:

$$\mathbf{D}_u = \begin{pmatrix} d_u^0(0) & d_u^1(0) & \cdots & d_u^{N_t-1}(0) \\ d_u^0(1) & d_u^1(1) & \cdots & d_u^{N_t-1}(1) \\ \vdots & \vdots & \ddots & \vdots \\ d_u^0(K-1) & d_u^1(K-1) & \cdots & d_u^{N_t-1}(K-1) \end{pmatrix}, \quad (1)$$

where $d_u^i(k) \in \{-1, 1\}$ represents the binary symbol transmitted by the uth user at transmit antenna i over time slot k. Since K time slots are required for N_b symbols transmission, the code rate is $R = N_b/K$. The transmitter converts the ith column of the ST codeword matrix into UWB signal which is then transmitted from the transmit antenna i. The resultant ST UWB signal can be expressed as an $K \times N_t$ matrix $\widetilde{\mathbf{X}}_u(t)$ whose (k, i)th element is the transmitted UWB signal $\tilde{x}_u^i(k; t)$ corresponding to the symbol $d_u^i(k)$. In general, UWB signal comprises short-length pulses, usually referred to as monocycles, with durations generally in the order of several nanoseconds (ns). The UWB signal also depends on particular MA and modulation techniques. Figure 2 illustrates an example of UWB signals employing TH-BPPM, TH-BPSK, and DS-BPSK schemes, which will be discussed in the following sections.

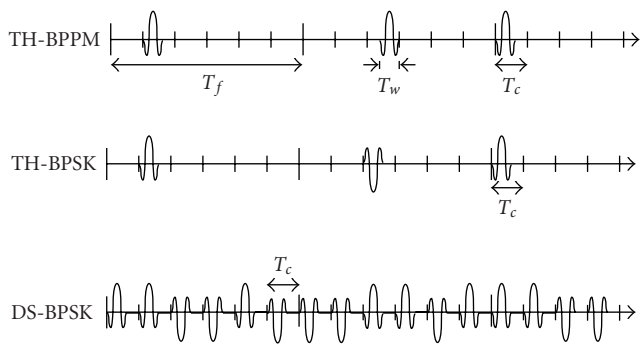

Figure 2: UWB signals with various modulation and MA techniques.

2.1. TH-BPPM

The conventional UWB modulation is based on TH-BPPM, in which the information is conveyed by the positions of the pulses. The uth user's transmitted waveform at the ith transmit antenna during the kth frame can be described as [11, 20]

$$\tilde{x}_u^i(k;t) = \sqrt{\frac{E_u}{N_t}}\,\tilde{w}\left(t - kT_f - c_u(k)T_c - \frac{1 - d_u^i(k)}{2}T_d\right), \quad (2)$$

where $\tilde{w}(t)$ denotes the transmitted monocycle of duration T_w, T_f represents the frame interval corresponding to one symbol transmission, T_c is the hop duration, and T_d denotes the modulation delay. $d_u^i(k)$ represents the transmitted binary symbol, that is, $d_u^i(k) \in \{-1, 1\}$, as introduced previously. Typically, T_f is hundred or thousand times longer than the pulse width. We normalize the monocycle waveform to have unit energy, and introduce the factor $\sqrt{E_u/N_t}$ to ensure that the total transmitted energy of the uth user is E_u during each frame interval, independent of the number of transmit antennas. To accommodate the TH sequences in MA environments, T_f is further divided into N_c segments of T_c seconds, where $N_cT_c \le T_f$. The TH sequence of the uth user is denoted by $\{c_u(k)\}$, $0 \le c_u(k) \le N_c - 1$. It provides an additional time shift of $c_u(k)T_c$ seconds to the kth monocycle in order to allow MA without catastrophic collisions. In a synchronized network, an orthogonal TH sequence that satisfies $c_u(k) \ne c_{u'}(k)$ for all k's and for any two users $u \ne u'$ can be adopted to minimize the interference with each other. Performance of synchronous MA systems using various TH sequences such as Gold sequence and simulated annealing code has been studied in [21]. For an asynchronous system, the choice of orthogonal TH sequence does not guarantee collision-free transmission [16]. In this paper, we utilize random TH sequence, where $c_u(k)$ is a discrete uniform random variable over the set $\{0, 1, \ldots, N_c - 1\}$, as in [15, 16, 18]. The modulation delay T_d is used to distinguish between pulses carrying information -1 and 1. Specifically, in addition to the frame and hop delays, the monocycle conveying information $d_u^i(k) = -1$ is shifted by a modulation delay of T_d seconds, whereas the monocycle carrying $d_u^i(k) = 1$ is transmitted without any additional delay. Since an interval of $T_w + T_d$ seconds is used for one symbol modulation, the hop duration is chosen to satisfy $T_c = T_w + T_d$.

2.2. TH-BPSK

TH-BPSK scheme exploits the same TH sequence concept as in the TH-BPPM. However, the information in TH-BPSK system is carried in the polarities of the pulses, rather than their time delays. The transmitted UWB-TH-BPSK signal is given by [12]

$$\tilde{x}_u^i(k;t) = \sqrt{\frac{E_u}{N_t}}\,d_u^i(k)\tilde{w}(t - kT_f - c_u(k)T_c). \quad (3)$$

Similar to the TH-BPPM case, each frame contains only one monocycle with a delay corresponding to the assigned TH sequence, $\{c_u(k)\}$, $0 \le c_u(k) \le N_c - 1$. Since the modulation interval is T_w, the hop duration is selected such that $T_c = T_w$. The monocycle is normalized to have unit energy, and the total transmitted energy per frame of the uth user is E_u.

2.3. DS-BPSK

In DS-BPSK systems, the binary symbol $d_u^i(k)$ to be transmitted over the kth frame interval is spread by a sequence of multiple monocycles $\{c_u(n_c)\tilde{w}(t - kT_f - n_cT_c)\}_{n_c=0}^{N_c-1}$, whose polarities are determined by the spreading sequence $\{c_u(n_c)\}_{n_c=0}^{N_c-1}$. Such a spreading sequence is uniquely assigned to each user in an MA system in order to allow multiple transmissions with little interference. Similar to the TH system, an orthogonal spreading sequence such as Gold sequence or Hadamard-Walsh code can be selected to mitigate multiple-access interference (MAI) in a synchronous network [13]. Considering an asynchronous system where orthogonal sequences do not guarantee the complete mitigation of MAI, we adopt the random spreading sequences in which $c_u(n_c)$ for different u and n_c take values from $\{-1, 1\}$ with equal probabilities [15, 16]. The transmitted DS-BPSK signal model can be described as [13, 14]

$$\tilde{x}_u^i(k;t) = \sqrt{\frac{E_u}{N_tN_c}}\,d_u^i(k)\sum_{n_c=0}^{N_c-1} c_u(n_c)\tilde{w}(t - kT_f - n_cT_c), \quad (4)$$

where $\tilde{w}(t)$ represents the monocycle whose energy is normalized. The frame interval T_f is divided into N_c segments of duration T_c, each containing a monocycle of length T_w. Therefore, the hop period is chosen to satisfy $T_c = T_w$. This condition results in the orthogonality between the monocycles contained in a sequence regardless of the particular spreading code, that is, $\int_{-\infty}^{\infty} c_u(n_c)\tilde{w}(t - kT_f - n_cT_c)c_u(n_c')\tilde{w}(t - k'T_f - n_c'T_c)dt = \delta(n_c - n_c')\delta(k - k')$. Since each frame contains N_c monocycles, we introduce the factor $\sqrt{1/N_c}$ to ensure that the sequence of N_c monocycles has unit energy. That is, $(1/N_c)\sum_{n_c=0}^{N_c-1}\int_{-\infty}^{\infty}[\tilde{w}(t - kT_f - n_cT_c)]^2dt = 1$. With the monocycle sequence being normalized and the factor $\sqrt{E_u/N_t}$ being included, the uth user's transmitted energy per frame is E_u.

3. UWB-MIMO RECEIVER PROCESSING

We consider frequency selective channel model [17], where the channel of the uth user is modelled as a tapped delay line with L_u taps. The channels are assumed to be real, mutually independent, and quasistatic, that is, the channels remain constant during one codeword transmission, and change independently from one codeword transmission to the next. The channel impulse response from the ith transmit antenna of the uth user to the jth receive antenna can be described as

$$h_u^{ij}(t) = \sum_{l=0}^{L_u-1} \alpha_u^{ij}(l)\delta(t-\tau_u(l)), \tag{5}$$

where $\alpha_u^{ij}(l)$ is the multipath gain coefficient, L_u denotes the number of resolvable paths, and $\tau_u(l)$ represents the path delay relative to the delay of the desired user's first arrival path. Therefore, without loss of generality, we consider the first user as the desired user, and assume that $\tau_0(0) = 0$. Here, we analyze an asynchronous MA system in which $\{\tau_u(0)\}_{u=1}^{N_u-1}$ are random variables derived from the uniform distribution. In order to simplify the analysis, we assume that the minimum resolvable delay is equal to the pulse width, as in [13]. This assumption infers that $\tau_u(l) - \tau_u(l-1) \geq T_w$ for any $l \in \{1, 2, \ldots, L_u - 1\}$. To avoid the intersymbol interference (ISI), we choose the signal parameters to satisfy

$$N_c T_c + \max_u \{\tau_u(L_u - 1)\} \leq T_f. \tag{6}$$

The amplitude of the lth path, $|\alpha_u^{ij}(l)|$, is modelled as a Nakagami-m random variable with a probability density function (pdf) [22]

$$p_{|\alpha_u^{ij}(l)|}(x) = \frac{2}{\Gamma(m)}\left(\frac{m}{\Omega_u(l)}\right)^m x^{2m-1}\exp\left(-\frac{m}{\Omega_u(l)}x^2\right), \tag{7}$$

where $\Gamma(\cdot)$ denotes the Gamma function, m is the fading parameter, and $\Omega_u(l) = \mathrm{E}[|\alpha_u^{ij}(l)|^2]$, with $\mathrm{E}[\cdot]$ representing the expectation operation, is the average power. We assume that for each user, the time delay $\{\tau_u(l)\}$ and the average power $\Omega_u(l)$ of the lth path are similar for every transmit-receive link. The fading parameter, m, can be any real value that satisfies $m \geq 1/2$. The smaller the m, the more severe the fading, with $m = 1$ and $m = \infty$ corresponding to the Rayleigh fading and nonfading channels.

The signal received at each receive antenna consists of multipath signals from all active users and thermal noise. Due to the effect of propagation channel and the variation of antenna characteristics caused by large bandwidth, the shape of the transmitted monocycle $\tilde{w}(t)$ is modified to its second derivative at the receive antenna output [18, 19]. Denoting the received monocycle waveform by $w(t)$ and applying the channel model in (5), the received signal at receive antenna j can be modelled as

$$r^j(t) = \sum_{u=0}^{N_u-1}\sum_{i=0}^{N_t-1}\sum_{k=0}^{K-1}\sum_{l=0}^{L_u-1} \alpha_u^{ij}(l)x_u^i(k; t-\tau_u(l)) + n^j(t), \tag{8}$$

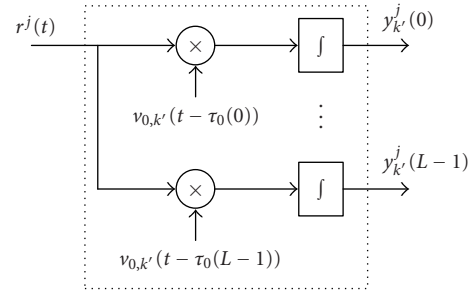

Figure 3: RAKE receiver at the jth received antenna.

where $x_u^i(k;t)$ is of the form similar to the transmitted waveform $\tilde{x}_u^i(k;t)$ by replacing $\tilde{w}(t)$ with $w(t)$, and $n^j(t)$ is real additive white Gaussian noise process with zero mean and two-sided power spectral density $N_0/2$. With the first user being the desired user, the received signal model in (8) can be reexpressed as

$$r^j(t) = \sum_{i=0}^{N_t-1}\sum_{k=0}^{K-1}\sum_{l=0}^{L_0-1} \alpha_0^{ij}(l)x_0^i(k; t-\tau_0(l)) + n_{\mathrm{MU}}^j(t) + n^j(t), \tag{9}$$

where

$$n_{\mathrm{MU}}^j(t) = \sum_{u=1}^{N_u-1}\sum_{i=0}^{N_t-1}\sum_{k=0}^{K-1}\sum_{l=0}^{L_u-1} \alpha_u^{ij}(l)x_u^i(k; t-\tau_u(l)) \tag{10}$$

is the signal received from other users.

For the signal transmitted from the desired user, we assume that the receiver has perfect synchronization and the knowledge of the TH or spreading sequence. We also assume that the desired user's channel state information (CSI) is known at the receiver but not at the transmitter. In addition, we assume that the received monocycle waveform $w(t)$ is known at the receiver. The autocorrelation function of $w(t)$ is given by

$$\gamma(s) = \int_{-\infty}^{\infty} w(t-s)w(t)ds, \tag{11}$$

where $\gamma(0) = 1$ and $\gamma(s)$ can be approximately zero when $|s| \geq T_w$, that is, the time difference between the monocycles is longer than the pulse duration. At the receiver, we employ L-finger ($L \leq \max_u\{L_u\}$) RAKE receivers, each adopting the delayed versions of the received monocycle as the reference waveform. Figure 3 illustrates an example of a RAKE receiver whose reference signal is denoted by $v_{0,k'}(t)$. We choose the finger delays such that the signals from the first L arriving paths are selected. The output of the l'th correlator at receive antenna j is given by

$$y_{k'}^j(l') = \int_{-\infty}^{\infty} v_{0,k'}(t-\tau_0(l'))r^j(t)dt. \tag{12}$$

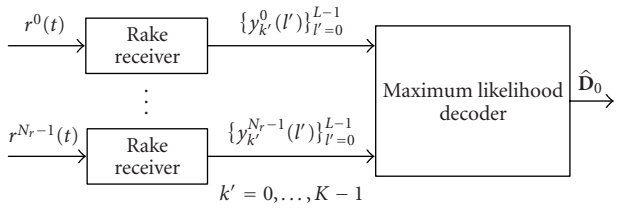

Figure 4: UWB-MIMO receiver description.

Substituting the received signal in (9) into (12), we have

$$\begin{aligned} y^j_{k'}(l') &= \sum_{i=0}^{N_t-1}\sum_{k=0}^{K-1}\sum_{l=0}^{L_0-1}\alpha_0^{ij}(l)\int_{-\infty}^{\infty} v_{0,k'}(t-\tau_0(l')) \\ &\qquad \times x_0^i(k; t-\tau_u(l))\,dt \\ &\quad + \int_{-\infty}^{\infty} v_{0,k'}(t-\tau_0(l'))\, n^j_{\mathrm{MU}}(t)\,dt \\ &\quad + \int_{-\infty}^{\infty} v_{0,k'}(t-\tau_0(l'))\, n^j(t)\,dt \\ &\triangleq y^j_{d,k'}(l') + \underbrace{n^j_{\mathrm{MU},k'}(l') + n^j_{k'}(l')}_{n^j_{\mathrm{tot},k'}(l')}, \end{aligned} \tag{13}$$

where $y^j_{d,k'}(l')$, $n^j_{\mathrm{MU},k'}(l')$, and $n^j_{k'}(l')$ denote the correlator outputs corresponding to the desired transmitted information, MAI, and thermal noise, respectively. Assuming no ISI, that is, (6) is satisfied, only the desired user's signal transmitted during the k'th frame will contribute to $y^j_{d,k'}(l')$. Thus, we can express $y^j_{d,k'}(l')$ in (13) as

$$\begin{aligned} y^j_{d,k'}(l') &= \sum_{i=0}^{N_t-1}\sum_{l=0}^{L_0-1}\alpha_0^{ij}(l) \\ &\qquad \times \int_{-\infty}^{\infty} v_{0,k'}(t-\tau_0(l'))\, x_0^i(k'; t-\tau_0(l))\,dt. \end{aligned} \tag{14}$$

The RAKE receivers are followed by a maximum likelihood (ML) decoder, where the decoding process is performed jointly across all N_r receive antennas, as shown in Figure 4. In what follows, we analyze the receiver assuming different modulation and MA techniques employed.

3.1. TH-BPPM

The design of TH-BPPM receiver depends on the choice of the modulation delay, T_d. Any choice of $T_d \geq T_w$ yields an equivalent design to orthogonal signalling scheme. However, due to the multipath propagation, such orthogonality can be corrupted at the receiver. To preserve the orthogonality, T_d has to satisfy the condition $T_d \geq \max_u\{\tau_u(L_u-1)\} + T_w$. This results in the loss of the transmission rate. In the followings, we choose T_d to minimize the correlation $\int_{-\infty}^{\infty} w(t)w(t-T_d)dt$, as in [11]. With this choice of T_d, the design is close to an antipodal signaling scheme, and the transmission rate can be made equal to the system with BPSK modulation. The correlation waveform adopted at each RAKE receiver is modelled as

$$\begin{aligned} v_{0,k'}(t) &= w(t-k'T_f - c_0(k')T_c) \\ &\quad - w(t-k'T_f - c_0(k')T_c - T_d). \end{aligned} \tag{15}$$

Substituting the transmitted signal in (2) and the reference waveform in (15) into (14), $y^j_{d,k'}(l')$ can be expressed as

$$\begin{aligned} y^j_{d,k'}(l') &= \sqrt{\frac{E_0}{N_t}}\sum_{i=0}^{N_t-1}\sum_{l=0}^{L_0-1}\alpha_0^{ij}(l) \\ &\qquad \times \int_{-\infty}^{\infty} w\Big(t-k'T_f - c_0(k')T_c \\ &\qquad\qquad - \frac{1-d_u^i(k')}{2}T_d - \tau_0(l)\Big) \\ &\qquad \times [w(t-k'T_f - c_0(k')T_c - \tau_0(l')) \\ &\qquad\quad - w(t-k'T_f - c_0(k')T_c - T_d \\ &\qquad\quad - \tau_0(l'))]\,dt. \end{aligned} \tag{16}$$

Using the definition of $\gamma(\cdot)$ in (11), (16) can be simplified to

$$\begin{aligned} y^j_{d,k'}(l') &= \sqrt{\frac{E_0}{N_t}}\sum_{i=0}^{N_t-1}\alpha_0^{ij}(l') \\ &\qquad \times \underbrace{\left[\gamma\left(\frac{1-d_0^i(k')}{2}T_d\right) - \gamma\left(\frac{1-d_0^i(k')}{2}T_d - T_d\right)\right]}_{\triangleq s_0^i(k')} \\ &\qquad + n^j_{p,k'}(l'), \end{aligned} \tag{17}$$

where

$$n^j_{p,k'}(l') \triangleq \sqrt{\frac{E_0}{N_t}}\sum_{i=0}^{N_t-1}\sum_{l=0,\,l\neq l'}^{L_0-1}\alpha_0^{ij}(l)\left\{\gamma\left[\tau_0(l)-\tau_0(l')+(1-d_0^i(k'))\frac{T_d}{2}\right] - \gamma\left[\tau_0(l)-\tau_0(l')+(1-d_0^i(k'))\frac{T_d}{2} - T_d\right]\right\}. \tag{18}$$

We show in the appendix that $n^j_{p,k'}(l')$ is negligible as long as $\tau_0(l) - \tau_0(l-1) \geq T_w$. Also, observe from (17) that $s^i_0(k') = 1 - \gamma(T_d)$ when $d^i_0(k') = 1$, whereas $s^i_0(k') = \gamma(T_d) - 1$ when $d^i_0(k') = -1$. Therefore, we can express $s^i_0(k')$ as $[1 - \gamma(T_d)]d^i_0(k')$. Replacing $s^i_0(k')$ in (17) with $[1 - \gamma(T_d)]d^i_0(k')$ and neglecting $n^j_{p,k'}(l')$, the expression of $y^j_{d,k'}(l')$ can be simplified to

$$y^j_{d,k'}(l') = [1 - \gamma(T_d)]\sqrt{\frac{E_0}{N_t}} \sum_{i=0}^{N_t-1} d^i_0(k')\alpha^{ij}_0(l'). \tag{19}$$

Finally, from (19) and (13), we can express the correlator output $y^j_{k'}(l')$ as

$$y^j_{k'}(l') = [1-\gamma(T_d)]\sqrt{\frac{E_0}{N_t}} \sum_{i=0}^{N_t-1} d^i_0(k')\alpha^{ij}_0(l') + n^j_{\text{tot},k'}(l'). \tag{20}$$

Expressing the correlator outputs in (20) in the matrix form, we have

$$\mathbf{Y}^j = [1 - \gamma(T_d)]\sqrt{\frac{E_0}{N_t}}\mathbf{D}_0\mathbf{A}^j_0 + \mathbf{N}^j_{\text{tot}}, \tag{21}$$

where $\mathbf{D}_0$ is the desired user's transmitted ST symbol defined in (1). Both matrices $\mathbf{Y}^j$ and $\mathbf{N}^j_{\text{tot}}$ are of size $K \times L$, whose (k,l)th elements are $y^j_k(l)$ and $n^j_{\text{tot},k}(l)$ (see (13)), respectively. The multipath gain coefficient matrix $\mathbf{A}^j_0$ of size $N_t \times L$ is formatted as

$$\mathbf{A}^j_0 = \begin{pmatrix} \alpha^{0j}_0(0) & \alpha^{0j}_0(1) & \cdots & \alpha^{0j}_0(L-1) \\ \alpha^{1j}_0(0) & \alpha^{1j}_0(1) & \cdots & \alpha^{1j}_0(L-1) \\ \vdots & \vdots & \ddots & \vdots \\ \alpha^{(N_t-1)j}_0(0) & \alpha^{(N_t-1)j}_0(1) & \cdots & \alpha^{(N_t-1)j}_0(L-1) \end{pmatrix}. \tag{22}$$

Given the CSI on MIMO channels, the decoder performs ML decoding by selecting a codeword $\hat{\mathbf{D}}_0$ which minimizes the square Euclidean distance between the hypothesized and actual correlator output matrices. The decision rule can be stated as

$$\hat{\mathbf{D}}_0 = \arg\min_{\mathbf{D}_0} \sum_{j=0}^{N_r-1} \left\| \mathbf{Y}^j - [1 - \gamma(T_d)]\sqrt{\frac{E_0}{N_t}}\mathbf{D}_0\mathbf{A}^j_0 \right\|^2, \tag{23}$$

where $\|\mathbf{X}\|$ denotes the Frobenius norm of an $M \times N$ matrix $\mathbf{X} = (x_{mn})$, defined by [23]

$$\|\mathbf{X}\| = \left(\sum_{m=0}^{M-1} \sum_{n=0}^{N-1} |x_{mn}|^2 \right)^{1/2}. \tag{24}$$

3.2. TH-BPSK

The reference waveform used at the TH-BPSK receiver is the delayed version of the received monocycle, that is,

$$v_{0,k'}(t) = w(t - k'T_f - c_0(k')T_c). \tag{25}$$

Substituting the TH-BPSK signal in (3) and the template signal in (25) into (14), we can evaluate $y^j_{d,k'}(l')$ as follows:

$$\begin{aligned} y^j_{d,k'}(l') &= \sqrt{\frac{E_0}{N_t}} \sum_{i=0}^{N_t-1} d^i_0(k') \sum_{l=0}^{L_0-1} \alpha^{ij}_0(l) \\ &\quad \times \int_{-\infty}^{\infty} w(t - k'T_f - c_0(k')T_c - \tau_0(l')) \\ &\qquad \times w(t - k'T_f - c_0(k')T_c - \tau_0(l))\,dt \\ &= \sqrt{\frac{E_0}{N_t}} \sum_{i=0}^{N_t-1} d^i_0(k') \sum_{l=0}^{L_0-1} \alpha^{ij}_0(l)\gamma(\tau_0(l) - \tau_0(l')). \end{aligned} \tag{26}$$

Assuming $\tau_0(l) - \tau_0(l-1) \geq T_w$ and $\gamma(s) = 0$ for any $|s| \geq T_w$, we have $\gamma(\tau_0(l) - \tau_0(l')) = \delta(l - l')$. Therefore, (26) can be simplified to

$$y^j_{d,k'}(l') = \sqrt{\frac{E_0}{N_t}} \sum_{i=0}^{N_t-1} d^i_0(k')\alpha^{ij}_0(l'). \tag{27}$$

Combining (13) and (27), and rewriting all L correlator outputs of each receive antenna in the matrix form, we obtain

$$\mathbf{Y}^j = \sqrt{\frac{E_0}{N_t}}\mathbf{D}_0\mathbf{A}^j_0 + \mathbf{N}^j_{\text{tot}}, \tag{28}$$

in which $\mathbf{Y}^j$, $\mathbf{A}^j_0$, and $\mathbf{N}^j_{\text{tot}}$ are in the same forms as the ones stated in (21). The decision rule for the ML decoder can be written similar to (23) as

$$\hat{\mathbf{D}}_0 = \arg\min_{\mathbf{D}_0} \sum_{j=0}^{N_r-1} \left\| \mathbf{Y}^j - \sqrt{\frac{E_0}{N_t}}\mathbf{D}_0\mathbf{A}^j_0 \right\|^2. \tag{29}$$

3.3. DS-BPSK

The DS-BPSK receiver adopts the monocycle sequence

$$v_{0,k'}(t) = \sqrt{\frac{1}{N_c}} \sum_{n'_c=0}^{N_c-1} c_0(n'_c)\, w(t - k'T_f - n'_cT_c) \tag{30}$$

as the reference waveform. The correlator output can be found by substituting (4) and (30) into (13). First, we

evaluate $y^j_{d,k'}(l')$ (see (14)) as follows:

$$\begin{aligned} y^j_{d,k'}(l') &= \sqrt{\frac{E_0}{N_t}} \sum_{i=1}^{N_t} d^i_0(k') \sum_{l=0}^{L_0-1} \alpha^{ij}_0(l) \\ &\quad \times \underbrace{\frac{1}{N_c} \sum_{n'_c=0}^{N_c-1} c_0(n'_c) \sum_{n_c=0}^{N_c-1} c_0(n_c)\, \gamma\big((n_c - n'_c)T_c + (\tau_0(l) - \tau_0(l'))\big)}_{\triangleq f_0(l,l')} \\ &= \sqrt{\frac{E_0}{N_t}} \sum_{i=0}^{N_t-1} d^i_0(k') \sum_{l=0}^{L_0-1} \alpha^{ij}_0(l) f_0(l,l'). \end{aligned} \tag{31}$$

Then, substituting (31) into (13), we arrive at

$$y^j_{k'}(l') = \sqrt{\frac{E_0}{N_t}} \sum_{i=0}^{N_t-1} d^i_0(k') \sum_{l=0}^{L_0-1} \alpha^{ij}_0(l) f_0(l,l') + n^j_{\mathrm{tot},k'}(l'), \tag{32}$$

which can be written in the matrix form as

$$\mathbf{Y}^j = \sqrt{\frac{E_0}{N_t}} \mathbf{D}_0 \mathbf{A}^j_0 \mathbf{F}_0 + \mathbf{N}^j_{\mathrm{tot}}, \tag{33}$$

where $\mathbf{F}_0$ is an $L_0 \times L$ matrix whose (l,l')th element is $f_0(l,l')$. The multipath gain coefficient matrix $\mathbf{A}^j_0$ of size $N_t \times L_0$ is of a form similar to (22). Subsequently, the decision rule can be stated as

$$\hat{\mathbf{D}}_0 = \arg\min_{\mathbf{D}_0} \sum_{j=0}^{N_r-1} \left\| \mathbf{Y}^j - \sqrt{\frac{E_0}{N_t}} \mathbf{D}_0 \mathbf{A}^j_0 \mathbf{F}_0 \right\|^2. \tag{34}$$

4. PERFORMANCE ANALYSIS

To analyze the performances of the three different systems discussed in the previous section, we first calculate the noise and interference statistics. Regarding $n^j_{k'}(l')$ defined in (13), we have

$$\mathrm{E}[n^j_{k'}(l')] = \int_{-\infty}^{\infty} v_{0,k'}(t - \tau_0(l'))\, \mathrm{E}[n^j(t)]\, dt = 0. \tag{35}$$

The variance of $n^j_{k'}(l')$ can be computed as

$$\begin{aligned} \mathrm{E}\Big[\,|n^j_{k'}(l')|^2\Big] &= \int_{-\infty}^{\infty}\int_{-\infty}^{\infty} v_{0,k'}(s - \tau_0(l')) \\ &\qquad \times v_{0,k'}(t - \tau_0(l'))\, \underbrace{\mathrm{E}[n^j(s) n^j(t)]}_{(N_0/2)\delta(s-t)}\, ds\, dt \\ &= \frac{N_0}{2} \int_{-\infty}^{\infty} \big[v_{0,k'}(t - \tau_0(l'))\big]^2 dt \triangleq \sigma^2_n. \end{aligned} \tag{36}$$

Hence, $n^j_{k'}(l')$ is a zero-mean Gaussian random variable with variance σ^2_n. Next, we investigate the distribution of MAI, $n^j_{\mathrm{MU},k'}(l')$. Defining

$$n^i_{u,k'}(l,l') \triangleq \int_{-\infty}^{\infty} v_{0,k'}(t - \tau_0(l'))\, x^i_u(t - \tau_u(l))\, dt, \tag{37}$$

$n^j_{\mathrm{MU},k'}(l')$ (defined in (13)) can be reexpressed as

$$n^j_{\mathrm{MU},k'}(l') = \sum_{u=1}^{N_u-1} \sum_{i=0}^{N_t-1} \sum_{l=0}^{L-1} \alpha^{ij}_u(l) n^i_{u,k'}(l,l'). \tag{38}$$

Using the same approach as in [18], one can show that $n^i_{u,k'}(l,l')$ is an approximately Gaussian random variable with zero mean and variance

$$\begin{aligned} \mathrm{E}\Big[\,|n^j_{u,m}(k)|^2\Big] &= \frac{E_u}{N_t} \frac{1}{T_f} \int_{-\infty}^{\infty} \left[\int_{-\infty}^{\infty} w(t-s) v(t)\, dt \right]^2 ds \\ &\triangleq \frac{E_u}{N_t} \sigma^2_a. \end{aligned} \tag{39}$$

Assuming independent Nakagami fading coefficients, the statistics of $n^j_{\mathrm{MU},k'}(l')$ can be evaluated as follows:

$$\begin{aligned} \mathrm{E}[n^j_{\mathrm{MU},k'}(l')] &= \sum_{u=1}^{N_u-1} \sum_{i=0}^{N_t-1} \sum_{l=0}^{L-1} \mathrm{E}[\alpha^{ij}_u(l)]\, \mathrm{E}[n^i_{u,k'}(l,l')] = 0, \\ \mathrm{E}\Big[\,|n^j_{\mathrm{MU},k'}(l')|^2\Big] &= \sum_{u=1}^{N_u-1} \sum_{i=0}^{N_t-1} \sum_{l=0}^{L-1} \underbrace{\mathrm{E}\Big[\,|\alpha^{ij}_u(l)|^2\Big]}_{=\Omega_u(l)} \underbrace{\mathrm{E}\Big[\,|n^i_{u,k'}(l,l')|^2\Big]}_{=(E_u/N_t)\sigma^2_a} \\ &= \sigma^2_a \sum_{u=1}^{N_u-1} E_u \sum_{l=0}^{L-1} \Omega_u(l). \end{aligned} \tag{40}$$

Applying the central limit theorem for sufficiently large L, N_t, and N_u, $n^j_{\mathrm{MU},k'}(l')$ can be approximated as a Gaussian random variable with zero mean and variance $\sigma^2_a \sum_{u=1}^{N_u-1} E_u \sum_{l=0}^{L-1} \Omega_u(l)$. Therefore, we can model the total noise and interference $n^j_{\mathrm{tot},k'}(l') = n^j_{\mathrm{MU},k'}(l') + n^j_{k'}(l')$ as a zero-mean Gaussian random variable with variance

$$\begin{aligned} \mathrm{E}\Big[\,|n^j_{\mathrm{tot},k'}(l')|^2\Big] &= \mathrm{E}\Big[\,|n^j_{\mathrm{MU},k'}(l')|^2\Big] + \mathrm{E}\Big[\,|n^j_{k'}(l')|^2\Big] \\ &= \sigma^2_a \sum_{u=1}^{N_u-1} E_u \sum_{l=0}^{L-1} \Omega_u(l) + \sigma^2_n \triangleq \sigma^2_{n_{\mathrm{tot}}}. \end{aligned} \tag{41}$$

Since the total noise and interference can be approximated with Gaussian distribution, PEP can be evaluated in a similar fashion as in the conventional narrowband MIMO system. Such PEP calculation relies on the detection rule which is different for distinct modulation and MA schemes. In addition, since both σ^2_n and σ^2_a (defined, respectively, in (36) and (39)) are in terms of the reference signal $v(t)$, their values and hence the statistics of $n^j_{\mathrm{tot},k'}(l')$ also depend on particular modulation and MA techniques. The PEP evaluation for TH-BPPM, TH-BPSK, and DS-BPSK will be given in the following sections.

4.1. TH-BPPM

Recalling the template signal in (15), we have

$$\int_{-\infty}^{\infty}\left[v_{0,k'}(t-\tau_0(l'))\right]^2 dt = \int_{-\infty}^{\infty}\left[w(t)-w(t-T_d)\right]^2 dt = 2\left[1-\gamma(T_d)\right]. \tag{42}$$

Substituting (42) into (36), the noise variance is found to be $\sigma_n^2 = [1-\gamma(T_d)]N_0$. Next, replacing $v(t)$ in (39) with $w(t) - w(t-T_d)$, the value of σ_a^2 can be evaluated as

$$\begin{aligned}\sigma_a^2 &= \frac{1}{T_f}\int_{-\infty}^{\infty}\left[\int_{-\infty}^{\infty} w(t-s)\left[w(t)-w(t-T_d)\right]dt\right]^2 ds \\ &= \frac{1}{T_f}\int_{-\infty}^{\infty}\left[\gamma^2(s)+\gamma^2(s-T_d)-2\gamma(s)\gamma(s-T_d)\right]ds \\ &\triangleq 2\left(\bar{\sigma}_a^2-\sigma_d^2\right),\end{aligned} \tag{43}$$

where $\bar{\sigma}_a^2 = (1/T_f)\int_{-\infty}^{\infty}\gamma^2(s)ds$ and $\sigma_d^2 = (1/T_f)\int_{-\infty}^{\infty}\gamma(s)\gamma(s-T_d)ds$. Therefore, using (41), the variance of $n_{\mathrm{tot},k'}^j(l')$ is given by

$$\sigma_{n_{\mathrm{tot}}}^2 = 2\left(\bar{\sigma}_a^2-\sigma_d^2\right)\sum_{u=1}^{N_u-1}E_u\sum_{l=0}^{L-1}\Omega_u(l)+\left[1-\gamma(T_d)\right]N_0. \tag{44}$$

Suppose that $\mathbf{D}_0$ and $\hat{\mathbf{D}}_0$ are two distinct transmitted ST codewords; following similar calculation steps as in [17], the PEP conditioned on the channel coefficient matrix $\mathbf{A}_0^j$ is given by

$$P\left(\mathbf{D}_0 \longrightarrow \hat{\mathbf{D}}_0 \mid \mathbf{A}_0^j\right) = Q\left(\sqrt{\frac{\rho}{2N_t}\sum_{j=0}^{N_r-1}\left\|\left(\mathbf{D}_0-\hat{\mathbf{D}}_0\right)\mathbf{A}_0^j\right\|^2}\right), \tag{45}$$

where $Q(x)$ is the Gaussian error function defined as

$$\begin{aligned}Q(x) &= \frac{1}{\sqrt{2\pi}}\int_x^{\infty}\exp\left(-\frac{s^2}{2}\right)ds, \\ \rho &= \frac{\left[1-\gamma(T_d)\right]^2E_0}{2\sigma_{n_{\mathrm{tot}}}^2}.\end{aligned} \tag{46}$$

Substituting (44) into (46), we obtain

$$\rho = \left[4\frac{\bar{\sigma}_a^2-\sigma_d^2}{\left[1-\gamma(T_d)\right]^2}\sum_{u=1}^{N_u-1}\frac{E_u}{E_0}\sum_{l=0}^{L-1}\Omega_u(l)+\frac{2N_0}{\left[1-\gamma(T_d)\right]E_0}\right]^{-1}. \tag{47}$$

Note that if all users have equal transmitted power $E_0 = E_1 = \cdots = E_{N_u-1} \triangleq E$, (47) becomes

$$\rho = \left[4\frac{\bar{\sigma}_a^2-\sigma_d^2}{\left[1-\gamma(T_d)\right]^2}\sum_{u=1}^{N_u-1}\sum_{l=0}^{L-1}\Omega_u(l)+\left(\frac{\left[1-\gamma(T_d)\right]E}{2N_0}\right)^{-1}\right]^{-1}. \tag{48}$$

Applying the inequality $Q(x) \le (1/2)\exp(-x^2/2)$, for $x > 0$, the conditional PEP in (45) can be upper bounded by

$$P\left(\mathbf{D}_0 \longrightarrow \hat{\mathbf{D}}_0 \mid \mathbf{A}_0^j\right) \le \frac{1}{2}\exp\left(-\frac{\rho}{4N_t}\sum_{j=0}^{N_r-1}\left\|\left(\mathbf{D}_0-\hat{\mathbf{D}}_0\right)\mathbf{A}_0^j\right\|^2\right). \tag{49}$$

For convenience, we define

$$\mathbf{Z} = \left(\mathbf{D}_0-\hat{\mathbf{D}}_0\right)^{\mathrm{T}}\left(\mathbf{D}_0-\hat{\mathbf{D}}_0\right), \tag{50}$$

where $(\cdot)^{\mathrm{T}}$ denotes transpose operation. The term $\|(\mathbf{D}_0 - \hat{\mathbf{D}}_0)\mathbf{A}_0^j\|^2$ in (49) can be expressed as

$$\left\|\left(\mathbf{D}_0-\hat{\mathbf{D}}_0\right)\mathbf{A}_0^j\right\|^2 = \sum_{l=0}^{L-1}\left(\mathbf{a}_0^j(l)\right)^{\mathrm{T}}\mathbf{Z}\mathbf{a}_0^j(l), \tag{51}$$

where $\mathbf{a}_0^j(l)$ denotes the lth column of $\mathbf{A}_0^j$. Since $\mathbf{Z}$ is a real symmetric matrix, there exists a set of nonnegative eigenvalues $\{\lambda_i\}_{i=0}^{N_t-1}$ and the corresponding normalized eigenvectors $\{\mathbf{v}_i\}_{i=0}^{N_t-1}$ such that

$$\mathbf{Z} = \mathbf{V}\mathbf{\Lambda}\mathbf{V}^{\mathrm{T}}, \tag{52}$$

where $\mathbf{V} \triangleq [\mathbf{v}_0\ \mathbf{v}_1\ \cdots\ \mathbf{v}_{N_t-1}]$ is an orthonormal matrix and $\mathbf{\Lambda}$ is a diagonal matrix whose diagonal elements are the eigenvalues of $\mathbf{Z}$. Substituting (52) into (51), we have

$$\begin{aligned}\left\|\left(\mathbf{D}_0-\hat{\mathbf{D}}_0\right)\mathbf{A}_0^j\right\|^2 &= \sum_{l=0}^{L-1}\left(\mathbf{a}_0^j(l)\right)^{\mathrm{T}}\mathbf{V}\mathbf{\Lambda}\mathbf{V}^{\mathrm{T}}\mathbf{a}_0^j(l) \\ &= \sum_{l=0}^{L-1}\sum_{i=0}^{N_t-1}\lambda_i\left|\beta^{ij}(l)\right|^2,\end{aligned} \tag{53}$$

in which $\beta^{ij}(l) \triangleq (\mathbf{a}_0^j(l))^{\mathrm{T}}\mathbf{v}_i$. Since $\{\alpha_0^{ij}(l)\}_{i=0}^{N_t-1}$ are independent and identically distributed (i.i.d.) and $\mathbf{V}$ is orthonormal, $\{\mathbf{v}_0, \mathbf{v}_1, \ldots, \mathbf{v}_{N_t-1}\}$ is an orthonormal basis of $\mathcal{R}^{N_t}$ and $\{\beta^{ij}(l)\}_{i=0}^{N_t-1}$ are independent random variables whose magnitude is approximately Nakagami-m distributed with parameter $\tilde{m} = N_t m/(N_t m - m + 1)$ and average power $\Omega_0(l)$ (see [22, page 25]). By the use of characteristic function, the pdf of $|\beta^{ij}(l)|^2$ is given by [24]

$$p_{|\beta^{ij}(l)|^2}(x) = \frac{1}{\Gamma(\tilde{m})}\left(\frac{\tilde{m}}{\Omega_0(l)}\right)^{\tilde{m}}x^{\tilde{m}-1}\exp\left(-\frac{\tilde{m}}{\Omega_0(l)}x\right). \tag{54}$$

Substituting (53) into (49) and averaging (49) with respect to the distribution of $|\beta^{ij}(l)|^2$, the resultant PEP upper bound can be found as

$$P\left(\mathbf{D}_0 \longrightarrow \hat{\mathbf{D}}_0\right) \le \left[\prod_{l=0}^{L-1}\prod_{i=0}^{N_t-1}\left(1+\frac{\rho}{4N_t}\frac{\Omega_0(l)}{\tilde{m}}\lambda_i\right)\right]^{-\tilde{m}N_r}. \tag{55}$$

For high signal-to-noise ratio (SNR) environments, the bound in (55) can be further simplified to

$$P(\mathbf{D}_0 \longrightarrow \hat{\mathbf{D}}_0) \le \left(\prod_{l=0}^{L-1}\prod_{i=0}^{r-1}\frac{\rho}{4N_t}\frac{\Omega_0(l)}{\widetilde{m}}\lambda_i\right)^{-\widetilde{m}N_r} = \left[G_0(\widetilde{m})\frac{\rho}{4N_t}\right]^{-\widetilde{m}rN_rL}, \tag{56}$$

where $G_0(\widetilde{m}) \triangleq (\widetilde{m})^{-1}(\prod_{l=0}^{L-1}\Omega_0(l))^{1/L}(\prod_{i=0}^{r-1}\lambda_i)^{1/r}$, r is the rank, and $\{\lambda_i\}_{i=0}^{r-1}$ represent nonzero eigenvalues of matrix $\mathbf{Z}$. For a single-user system, since there is no effect of MAI, ρ in (48) reduces to $[1-\gamma(T_d)]E_0/2N_0$. Thus, the PEP upper bound in (56) becomes

$$P(\mathbf{D}_0 \longrightarrow \hat{\mathbf{D}}_0) \le \left[G_0(\widetilde{m})\frac{[1-\gamma(T_d)]E_0}{8N_tN_0}\right]^{-\widetilde{m}rN_rL}. \tag{57}$$

In this case, the exponent $\widetilde{m}rN_rL$ determines the slope of the performance curve plotted as a function of SNR, whereas the product $G_0(\widetilde{m})$ displaces the curve. Hence, the minimum values of $\widetilde{m}rN_rL$ and $G_0(\widetilde{m})$ over all pairs of distinct codewords define the diversity gain and the coding gain, respectively. Note that $r \le N_t$; therefore, the maximum achievable diversity gain is $\widetilde{m}N_tN_rL$.

4.2. TH-BPSK

Since the reference signal for the TH-BPSK system is the shifted monocycle whose energy is unity, that is, $\int_{-\infty}^{\infty}[v_{0,k'}(t-\tau_0(l'))]^2dt = \int_{-\infty}^{\infty}[w(t)]^2dt = 1$, the noise variance becomes $\sigma_n^2 = N_0/2$. In addition, substituting $v(t) = w(t)$ in (39), we have $\sigma_a^2 = \bar{\sigma}_a^2$, where $\bar{\sigma}_a^2$ is defined in (43). Therefore, $n_{\text{tot},k'}^j(l')$ is a zero-mean Gaussian random variable with variance

$$\sigma_{n_{\text{tot}}}^2 = \bar{\sigma}_a^2\sum_{u=1}^{N_u-1}E_u\sum_{l=0}^{L-1}\Omega_u(l) + \frac{N_0}{2}. \tag{58}$$

As a result, following the same calculations as in the preceding section, the upper bound of the PEP can be expressed similar to (56) as

$$P(\mathbf{D}_0 \longrightarrow \hat{\mathbf{D}}_0) \le \left[G_0(\widetilde{m})\frac{\rho}{4N_t}\right]^{-\widetilde{m}rN_rL}, \tag{59}$$

where $G_0(\widetilde{m})$ is of the same form as the one defined in (56), and

$$\rho = \frac{E_0}{2\sigma_{n_{\text{tot}}}^2} = \left[2\bar{\sigma}_a^2\sum_{u=1}^{N_u-1}\frac{E_u}{E_0}\sum_{l=0}^{L-1}\Omega_u(l) + \left(\frac{E_0}{N_0}\right)^{-1}\right]^{-1}, \tag{60}$$

which becomes E_0/N_0 for the single-user system.

4.3. DS-BPSK

With the spreading sequence $\{c_u(n_c)\} \in \{-1, 1\}$ being i.i.d. discrete uniform random variables, the variance of $n_{k'}^j(l')$ can be found from (30) and (36) as

$$\begin{aligned}\sigma_n^2 &= \frac{N_0}{2}\frac{1}{N_c}\int_{-\infty}^{\infty}\mathrm{E}\left[\sum_{n_c'=0}^{N_c-1}c_0(n_c')w(t-k'T_f-n_c'T_c)\right]^2dt \\ &= \frac{N_0}{2}\frac{1}{N_c}\sum_{n_c'=0}^{N_c-1}\int_{-\infty}^{\infty}[w(t-k'T_f-n_c'T_c)]^2dt = \frac{N_0}{2}.\end{aligned} \tag{61}$$

Substituting (30) into (39) results in

$$\begin{aligned}\sigma_a^2 &= \frac{1}{T_f}\int_{-\infty}^{\infty}\left[\sqrt{\frac{1}{N_c}}\sum_{n_c'=0}^{N_c-1}c_0(n_c')\right. \\ &\qquad \left.\times\int_{-\infty}^{\infty}w(t-s)w(t-n_c'T_c)dt\right]^2ds \\ &= \frac{1}{T_f}\frac{1}{N_c}\sum_{n_c'=0}^{N_c-1}\int_{-\infty}^{\infty}\gamma^2(s)ds = \bar{\sigma}_a^2.\end{aligned} \tag{62}$$

Observe that both σ_n^2 and σ_a^2 for DS-BPSK are of the same values as those for TH-BPSK. Hence, the variance of $n_{\text{tot},k'}^j(l')$ can be expressed similar to (58). As with the case of TH-BPSK, the upper bound of the PEP conditioned on the channel matrix is given by

$$P(\mathbf{D}_0 \longrightarrow \hat{\mathbf{D}}_0 \mid \mathbf{A}_0^j) \le \frac{1}{2}\exp\left(-\frac{\rho}{4N_t}\sum_{j=0}^{N_r-1}\left|\left|(\mathbf{D}_0-\hat{\mathbf{D}}_0)\mathbf{A}_0^j\mathbf{F}_0\right|\right|^2\right), \tag{63}$$

where $\rho = E_0/(2\sigma_{n_{\text{tot}}}^2)$ is in the same form as in (60). The term $\|(\mathbf{D}_0 - \hat{\mathbf{D}}_0)\mathbf{A}_0^j\mathbf{F}_0\|^2$ can be evaluated as follows:

$$\left|\left|(\mathbf{D}_0-\hat{\mathbf{D}}_0)\mathbf{A}_0^j\mathbf{F}_0\right|\right|^2 = \mathrm{tr}\left(\mathbf{F}_0^{\mathrm{T}}(\mathbf{A}_0^j)^{\mathrm{T}}\mathbf{Z}\mathbf{A}_0^j\mathbf{F}_0\right), \tag{64}$$

where $\mathbf{Z}$ is defined in (50), and $\mathrm{tr}(\cdot)$ denotes the trace operation, that is, $\mathrm{tr}(\mathbf{X})$ is the sum of diagonal elements of $\mathbf{X}$. By the use of eigenvalue decomposition as in (52), we have

$$\begin{aligned}\left|\left|(\mathbf{D}_0-\hat{\mathbf{D}}_0)\mathbf{A}_0^j\mathbf{F}_0\right|\right|^2 &= \mathrm{tr}\left(\mathbf{F}_0^{\mathrm{T}}(\mathbf{A}_0^j)^{\mathrm{T}}\mathbf{V}\boldsymbol{\Lambda}\mathbf{V}^{\mathrm{T}}\mathbf{A}_0^j\mathbf{F}_0\right) \\ &= \mathrm{tr}\left(\mathbf{F}_0^{\mathrm{T}}(\mathbf{B}_0^j)^{\mathrm{T}}\boldsymbol{\Lambda}\mathbf{B}_0^j\mathbf{F}_0\right),\end{aligned} \tag{65}$$

in which $\mathbf{B}_0^j \triangleq \mathbf{V}^{\mathrm{T}}\mathbf{A}_0^j$ is an $N_t \times L_0$ matrix, whose (i,l)th element is $\beta^{ij}(l)$, as defined in the TH-UWB case. Since $\mathbf{V}$ is an orthonormal matrix and the elements of $\mathbf{A}_0^j$ at each column are Nakagami-m i.i.d., $\{\beta^{ij}(l)\}$ are independent. Define $\widetilde{\mathbf{B}}_0^j = \mathbf{B}_0^j\mathbf{F}_0$ and denote its (i,l')th element by $\widetilde{\beta}^{ij}(l')$, that is, $\widetilde{\beta}^{ij}(l') = \sum_{l=0}^{L_0-1}\beta^{ij}(l)f_0(l,l')$. We can simplify (65) to

$$\left|\left|(\mathbf{D}_0-\hat{\mathbf{D}}_0)\mathbf{A}_0^j\mathbf{F}_0\right|\right|^2 = \mathrm{tr}\left((\widetilde{\mathbf{B}}_0^j)^{\mathrm{T}}\boldsymbol{\Lambda}\widetilde{\mathbf{B}}_0^j\right) = \sum_{l=0}^{L-1}\sum_{i=0}^{N_t-1}\lambda_i\left|\widetilde{\beta}^{ij}(l)\right|^2. \tag{66}$$

Thus, the conditioned PEP upper bound in (63) can be expressed as

$$P(\mathbf{D}_0 \longrightarrow \hat{\mathbf{D}}_0 \mid \mathbf{A}_0^j) \le \frac{1}{2}\exp\left(-\frac{\rho}{4N_t}\sum_{j=0}^{N_r-1}\sum_{l=0}^{L-1}\sum_{i=0}^{N_t-1}\lambda_i\left|\widetilde{\beta}^{ij}(l)\right|^2\right). \tag{67}$$

The PEP upper bound can be found by averaging (67) with respect to the joint distribution of $\{|\widetilde{\beta}^{ij}(l)|^2\}$. Since $\{|\widetilde{\beta}^{ij}(l)|\}_{l=0}^{L-1}$ are correlated Nakagami random variables, their joint distribution is difficult to obtain. Therefore, instead of evaluating the average PEP upper bound directly, we quantify the performance merits of DS-UWB ST system by investigating the term $\sum_{j=0}^{N_r-1}\|(\mathbf{D}_0-\hat{\mathbf{D}}_0)\mathbf{A}_0^j\mathbf{F}_0\|^2$ as follows.

We first define $\Delta = \mathbf{I}_{N_rL}\otimes\mathbf{\Lambda}$, where $\mathbf{I}_x$ is the identity matrix of size $x\times x$, and $\otimes$ denotes the tensor product. Denote the vector operation as $\mathrm{vec}(\mathbf{X}) = [\mathbf{x}_0^{\mathrm{T}}\ \mathbf{x}_1^{\mathrm{T}}\ \cdots\ \mathbf{x}_{N-1}^{\mathrm{T}}]^{\mathrm{T}}$, in which $\mathbf{x}_n$ is the nth column of $\mathbf{X}$, and define a column vector $\widetilde{\mathbf{b}} \triangleq [(\mathrm{vec}(\widetilde{\mathbf{B}}_0^0))^{\mathrm{T}}\ (\mathrm{vec}(\widetilde{\mathbf{B}}_0^1))^{\mathrm{T}}\ \cdots\ (\mathrm{vec}(\widetilde{\mathbf{B}}_0^{N_r-1}))^{\mathrm{T}}]^{\mathrm{T}}$ of length N_tN_rL. Then it follows from (66) that

$$\sum_{j=0}^{N_r-1}\left\|(\mathbf{D}_0-\hat{\mathbf{D}}_0)\mathbf{A}_0^j\mathbf{F}_0\right\|^2 = \sum_{j=0}^{N_r-1}\mathrm{tr}\left((\widetilde{\mathbf{B}}_0^j)^{\mathrm{T}}\mathbf{\Lambda}\widetilde{\mathbf{B}}_0^j\right) = \widetilde{\mathbf{b}}^{\mathrm{T}}\Delta\widetilde{\mathbf{b}}. \tag{68}$$

Now, we can rewrite (63) as

$$P(\mathbf{D}_0 \longrightarrow \hat{\mathbf{D}}_0 \mid \mathbf{A}_0^j) \le \frac{1}{2}\exp\left(-\frac{\rho}{4N_t}\widetilde{\mathbf{b}}^{\mathrm{T}}\Delta\widetilde{\mathbf{b}}\right). \tag{69}$$

Let $\mathbf{R} = \mathrm{E}[\widetilde{\mathbf{b}}\widetilde{\mathbf{b}}^{\mathrm{T}}]$ denote the correlation matrix of $\widetilde{\mathbf{b}}$. Since the correlation matrix is nonnegative definite, it has a symmetric square root $\mathbf{U}$ such that $\mathbf{R} = \mathbf{U}^{\mathrm{T}}\mathbf{U}$ [23]. Let $\mathbf{q} = (\mathbf{U}^{\mathrm{T}})^{-1}\widetilde{\mathbf{b}}$. Since the correlation matrix of $\mathbf{q}$ is

$$\mathrm{E}[\mathbf{q}\mathbf{q}^{\mathrm{T}}] = \mathrm{E}\left[(\mathbf{U}^{\mathrm{T}})^{-1}\widetilde{\mathbf{b}}\widetilde{\mathbf{b}}^{\mathrm{T}}\mathbf{U}^{-1}\right] = (\mathbf{U}^{\mathrm{T}})^{-1}\mathbf{R}\mathbf{U}^{-1} = \mathbf{I}_{N_tN_rL}, \tag{70}$$

the components of $\mathbf{q}$ are uncorrelated. Substituting $\widetilde{\mathbf{b}} = \mathbf{U}^{\mathrm{T}}\mathbf{q}$ into (69), we arrive at

$$P(\mathbf{D}_0 \longrightarrow \hat{\mathbf{D}}_0 \mid \mathbf{A}_0^j) \le \frac{1}{2}\exp\left(-\frac{\rho}{4N_t}\mathbf{q}^{\mathrm{T}}\mathbf{U}\Delta\mathbf{U}^{\mathrm{T}}\mathbf{q}\right). \tag{71}$$

Assuming that $\mathbf{R}$ is of full rank, $\mathbf{U}$ is also of full rank [23]. Therefore, with the same argument as in the case of TH-UWB by replacing $\mathbf{Z}$ with $\mathbf{U}\Delta\mathbf{U}^{\mathrm{T}}$, it follows that the maximum diversity gain can be achieved by maximizing the rank of Δ. Note that

$$\mathrm{rank}(\Delta) = N_rL\,\mathrm{rank}(\mathbf{\Lambda}) = N_rL\,\mathrm{rank}(\mathbf{Z}), \tag{72}$$

where $\mathrm{rank}(\mathbf{X})$ stands for the rank of $\mathbf{X}$. Hence, the rank criterion for the DS-UWB ST system is identical to that of TH-UWB ST system. That is, the diversity gain can be maximized when $\mathbf{Z}$ is of full rank. In order to quantify the coding gain, it might be necessary to evaluate the statistics of $\mathbf{q}$ which is difficult to obtain for Nakagami fading distribution. In Section 6, we perform simulations to further investigate the performance of the DS-UWB ST system.

5. UWB-ST CODES USING REAL ROD

In this section, we consider two-transmit-antenna system employing ROD-ST coding scheme [6]. Generalization to UWB-ST systems with higher number of transmit antennas is straightforward.

Exploiting full-rate ROD code, the 2×2 ST codeword matrix $\mathbf{D}$ is given by

$$\mathbf{D} = \begin{pmatrix} d^0 & d^1 \\ -d^1 & d^0 \end{pmatrix}, \tag{73}$$

where the user subscript u is omitted for notation simplicity. Since two data symbols, d^0 and d^1, are transmitted over two frame intervals, the code is of full rate $R = 1$. In the sequel, we will show that for single-user UWB-ST systems, reducing the transmission rate does not result in further diversity gain. However, for multiuser systems, this is not the case, and we can gain more diversity by using reduced rates signals. For this reason, we will consider the UWB-ST codes constructed from ROD with rate $R = 1/K$, where $K \ge 2$ is an even integer. In this case, the ST codeword $\mathbf{D}$ is a $K\times 2$ matrix:

$$\mathbf{D} = d\left(\begin{pmatrix} 1 & 1 \\ -1 & 1 \end{pmatrix}^{\mathrm{T}}\cdots\begin{pmatrix} 1 & 1 \\ -1 & 1 \end{pmatrix}^{\mathrm{T}}\right)^{\mathrm{T}}_{K\times 2}, \tag{74}$$

that is, the data symbol d is transmitted repeatedly over K frames from both transmit antennas.

To evaluate the system performance, we determine the eigenvalues of the matrix $\mathbf{Z}$ defined in Section 4 as follows. In the case of full-rate ROD code, the corresponding matrix $\mathbf{Z}$ (see (50)) can be determined as

$$\mathbf{Z} = \sum_{i=0}^{1}(d^i-\hat{d}^i)^2\mathbf{I}_2 = 4\sum_{i=0}^{1}\delta(d^i-\hat{d}^i)\mathbf{I}_2. \tag{75}$$

Assuming that $\mathbf{D}$ and $\hat{\mathbf{D}}$ are two distinct codewords, $\mathbf{Z}$ is of full rank $r = 2$ and its nonzero eigenvalues are $\lambda_0 = \lambda_1 = 4\sum_{i=0}^{1}\delta(d^i-\hat{d}^i)$. Consequently, UWB-ROD-ST code can offer full diversity of $\widetilde{m}N_tN_rL$. For $(1/K)$-rate ROD-ST code, we have

$$\mathbf{Z} = (d-\hat{d})^2K\mathbf{I}_2 = 4K\delta(d-\hat{d})\mathbf{I}_2. \tag{76}$$

We observe from (76) that utilizing reduced-rate ROD code, $\mathbf{Z}$ is also of full rank with two equal eigenvalues $\lambda_i = 4K\delta(d-\hat{d})$, and therefore the maximum diversity gain of $\widetilde{m}N_tN_rL$ can be achieved.

From the above investigation, we can see that employing UWB-ROD-ST signal for two-transmit-antenna system results in two equal eigenvalues $\lambda_0 = \lambda_1 \triangleq \lambda$, and the matrix $\mathbf{Z} = \lambda \mathbf{I}_2$ of full rank $r = 2$. Substituting two equal eigenvalues into (55), the PEP upper bound can be simplified to

$$P(\mathbf{D} \longrightarrow \hat{\mathbf{D}}) \leq \left[\prod_{l=0}^{L-1} \left(1 + \frac{\Omega(l)}{\tilde{m}} \frac{\rho\lambda}{8} \right) \right]^{-2\tilde{m}N_r}, \quad (77)$$

where $\tilde{m} = 2m/(m+1)$. With channel parameters and N_r being fixed, (77) depends only on the value of $\rho\lambda$. The higher the $\rho\lambda$, the better the performance.

To compare the performance of various modulation systems utilizing both full- and reduced-rate ROD-ST codes, we assume that the energy per bit E_b is fixed. For simplicity, we also assume that all users have equal transmitted energy per frame (E). Expressing E in terms of E_b, we have $E = E_b$ for full-rate and $E = E_b/K$ for $(1/K)$-rate ROD-ST codes. Next, we observe from the previous calculations that employing similar modulation schemes and assuming one erroneous symbol, the eigenvalues for $(1/K)$-rate ROD code are K times larger than those for full-rate code. We denote the eigenvalue of full-rate ROD-ST system as $\bar{\lambda}$.

We first look at the single-user case. Considering a single-user TH-BPPM system with $\rho = [1 - \gamma(T_d)]E/2N_0$, we have

$$\rho\lambda = \frac{[1 - \gamma(T_d)]E_b}{2N_0} \bar{\lambda} \quad (78)$$

for full-rate and

$$\rho\lambda = \frac{[1 - \gamma(T_d)]E_b}{2KN_0} K\bar{\lambda} = \frac{[1 - \gamma(T_d)]E_b}{2N_0} \bar{\lambda} \quad (79)$$

for $(1/K)$-rate ROD code. Similarly, for BPSK modulation where $\rho = E/N_0$, we can show that

$$\rho\lambda = \frac{E_b}{N_0} \bar{\lambda} \quad (80)$$

for both full-rate and $(1/K)$-rate ROD codes. Since exploiting ROD code of different rates yields the same value of $\rho\lambda$, reducing the code rate does not improve the performance of single-user systems. Comparing (78) and (80), we observe that for both full- and reduced-rate codes, $\rho\lambda$ of TH-BPSK and DS-BPSK systems are $2[1 - \gamma(T_d)]^{-1}$ times that of TH-BPPM system. Since $[1 - \gamma(T_d)] < 2$, both TH-BPSK and DS-BPSK tend to outperform TH-BPPM system for every code rate.

For the multiuser case, considering TH-BPPM system for which ρ is computed in (48), we obtain

$$\rho\lambda = \left[4 \frac{\bar{\sigma}_a^2 - \sigma_d^2}{[1 - \gamma(T_d)]^2} \sum_{u=1}^{N_u - 1} \sum_{l=0}^{L-1} \Omega_u(l) + \left(\frac{[1 - \gamma(T_d)]E_b}{2N_0} \right)^{-1} \right]^{-1} \bar{\lambda} \quad (81)$$

for full-rate, and

$$\rho\lambda = \left[\frac{4}{K} \frac{\bar{\sigma}_a^2 - \sigma_d^2}{[1 - \gamma(T_d)]^2} \sum_{u=1}^{N_u - 1} \sum_{l=0}^{L-1} \Omega_u(l) + \left(\frac{[1 - \gamma(T_d)]E_b}{2N_0} \right)^{-1} \right]^{-1} \bar{\lambda} \quad (82)$$

for ROD-ST codes with $(1/K)$-rate. Unlike the single-user system, here $\rho\lambda$ for full rate is less than that of reduced rate. Thus, reducing the code rate is likely to improve multiuser system performance. Similar conclusion can be obtained for the BPSK system, whose $\rho\lambda$ for full-rate and $(1/K)$-rate ROD codes can be written respectively as

$$\rho\lambda = \left[2\bar{\sigma}_a^2 \sum_{u=1}^{N_u - 1} \sum_{l=0}^{L-1} \Omega_u(l) + \left(\frac{E_b}{N_0} \right)^{-1} \right]^{-1} \bar{\lambda}, \quad (83)$$

and

$$\rho\lambda = \left[\frac{2}{K} \bar{\sigma}_a^2 \sum_{u=1}^{N_u - 1} \sum_{l=0}^{L-1} \Omega_u(l) + \left(\frac{E_b}{N_0} \right)^{-1} \right]^{-1} \bar{\lambda}. \quad (84)$$

We now compare $\rho\lambda$ of TH-BPPM and TH/DS-BSPK multiuser systems employing ROD code with the same rate. In addition to the difference between desired user's energy of $2[1 - \gamma(T_d)]^{-1}$, the first term in the right-hand side of (83), which results from the effect of MAI, is $(1/2)(1 - \sigma_d^2/\bar{\sigma}_a^2)^{-1}[1 - \gamma(T_d)]^2$ times that of (81). This factor can make BPSK system more vulnerable to the MAI than BPPM system, as we will show by simulation results in the succeeding section.

6. SIMULATION RESULTS

To support the analytical results for both single and multiple user systems given in the previous sections, we perform simulations for UWB MA systems based on TH-BPPM, TH-BPSK, and DS-BPSK modulation schemes. We employ UWB signals with frame interval $T_f = 100$ nanoseconds and pulse duration T_w of 0.8 nanosecond. We adopt the Gaussian monocycle as the transmitted pulse. To accommodate the effect of propagation channel and the variation of antenna characteristics caused by a large frequency bandwidth, the received monocycle is modelled as the second derivative of the Gaussian pulse [18] as follows:

$$w(t) = \sqrt{\frac{8}{3}} (1 - 4\eta) \exp(-2\eta), \quad (85)$$

where $\eta = \pi(t/\tau_o)^2$ and τ_o ($\tau_o \approx 0.4T_w$) parameterizes the width of the monocycle. The factor $\sqrt{8/3}$ is introduced such that each monocycle has unit energy. The autocorrelation function of the pulse in (85) is given by [25]

$$\gamma(t) = \left(1 - 4\eta + \frac{4}{3}\eta^2 \right) \exp(-\eta). \quad (86)$$

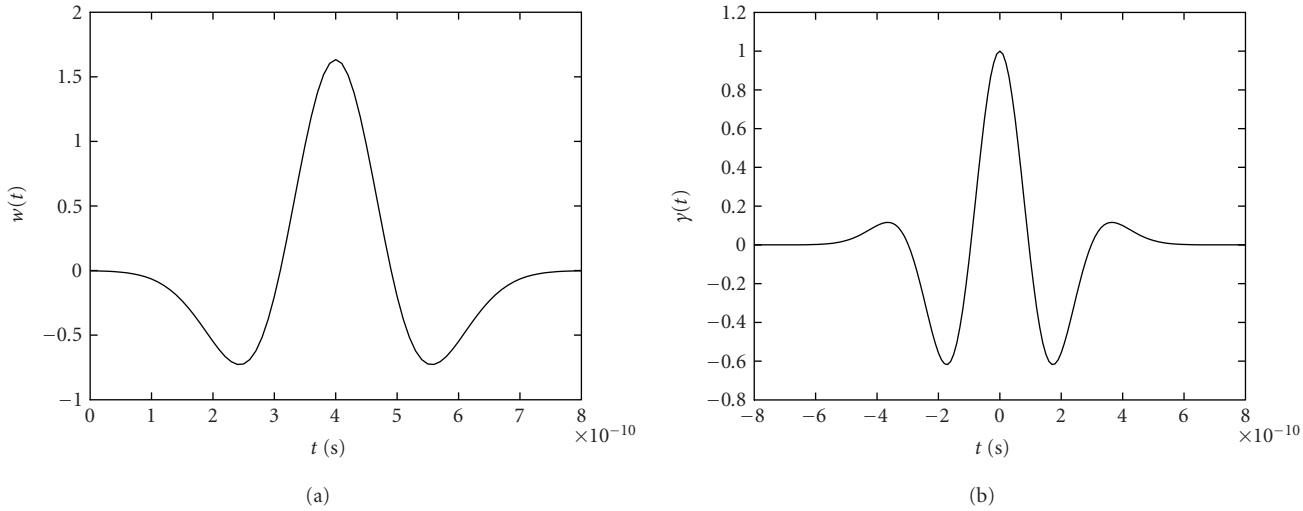

Figure 5: (a) The second derivative of the Gaussian monocycle waveform used at the receiver and (b) its autocorrelation function.

The second derivative of the Gaussian monocycle and its normalized autocorrelation function are shown in Figures 5a and 5b, respectively. Note that for a single-user system, utilizing rectangular monocycle, whose autocorrelation function is zero for $|t| \geq T_w$, yields the same performance as using the second derivative of Gaussian pulse. Therefore, $\gamma(t)$ in (86) can be approximately zero for $|t| \geq T_w$.

The transmitted data is a binary symbol taking value from $\{-1, 1\}$ with equal probability. In the TH-BPPM system, the modulation delay $T_d = \arg\min_{T_d} \int_{-\infty}^{\infty} w(t)w(t - T_d) = 0.22T_w$. Since an interval of $T_w + T_d$ seconds is required for one symbol modulation, we choose the hop duration $T_c = T_w + T_d$ seconds. Unlike the TH-BPPM, TH / DS-BPSK system does not require an additional time delay for data modulation, and hence its modulation interval can be made equal to the pulse duration. Therefore, the hop periods for both TH-BPSK and DS-BPSK systems are selected to be $T_c = T_w$. To avoid ISI, the total hop interval is limited to $N_c T_c \leq T_f - \max_u\{\tau_u(L_u - 1)\}$. Note that with a fixed T_f, since the hop duration of BPPM is larger than that of BPSK, BPPM can support less number of hops than the BPSK system. In order to evaluate the performance of an asynchronous system regardless of the choice of the particular code, both TH sequence and DS spreading are selected randomly [15, 16]. Here, the TH sequence equally takes the values from $\{0, 1, \ldots, N_c - 1\}$, whereas the spreading sequence $\{c_u(n_c)\}_{n_c=0}^{N_c-1} \in \{-1, 1\}$ with equal probability.

In this section, we show the performances of UWB ROD-ST block codes with different rates for real frequency-selective fading channels. The channels are quasistatic over K symbol periods. We employ the STDL channel model in which the delay profile is generated according to [26], and the path amplitude is Nakagami-m distributed with $m = 2$. The power of the L_u paths are normalized such that $\sum_{l=0}^{L_u-1} \Omega_u(l) = 1$. We assume that the power delay profiles of all users are similar. The thermal noise is a real Gaussian random process with zero mean and variance $N_0/2$. The channel coefficients, transmitted signals, and noise are generated independently. Unless specified otherwise, the number of fingers for the RAKE receiver is fixed to be $L = 4$.

Figures 6a and 6b show the BER performance of TH- and DS-UWB systems in single-user and multiuser environments. We can see from both figures that MIMO systems outperform SISO systems, and increasing the number of receive antennas yields better performance, regardless of the modulation and MA techniques. Consider the single-user case illustrated in Figure 6a. At any fixed SNR, the performances of TH-BPSK and DS-BPSK systems are close to each other, and both BPSK systems yield superior performances to the TH-BPPM. This observation is consistent with the theoretical results given in Section 5, which says that the value of $\rho\lambda$ for TH-BPSK and DS-BPSK systems are $2[1 - \gamma(T_d)]^{-1}$, and therefore their performances are better than that of the TH-BPPM system. In Figure 6b, we show the system performances when 5 asynchronous users are active. In low-SNR regime, the simulation results are similar to the single-user case. That is, TH-BPSK and DS-BPSK outperform the TH-BPPM scheme, and both BPSK systems yield close performances. However, due to the MAI, the BER of TH multiuser systems slightly drop with increasing E_b/N_0, and a high error floor can be noticed at high-SNR. This is due to the fact that in high-SNR regime, it is the effect of multiuser interference that prevails, regardless of the E_b/N_0. We can also observe from Figure 6b that the performance of TH-BPSK degrades faster than that of TH-BPPM. This means that at high SNR, TH-BPSK is more vulnerable to the MAI than the TH-BPPM system. On the other hand, even in MA scenarios, we can still see considerable improvement of the DS-BPSK-ST system. Therefore, it is evident that among the analyzed schemes, the DS-BPSK-ST system provides the best performance in MA environments.

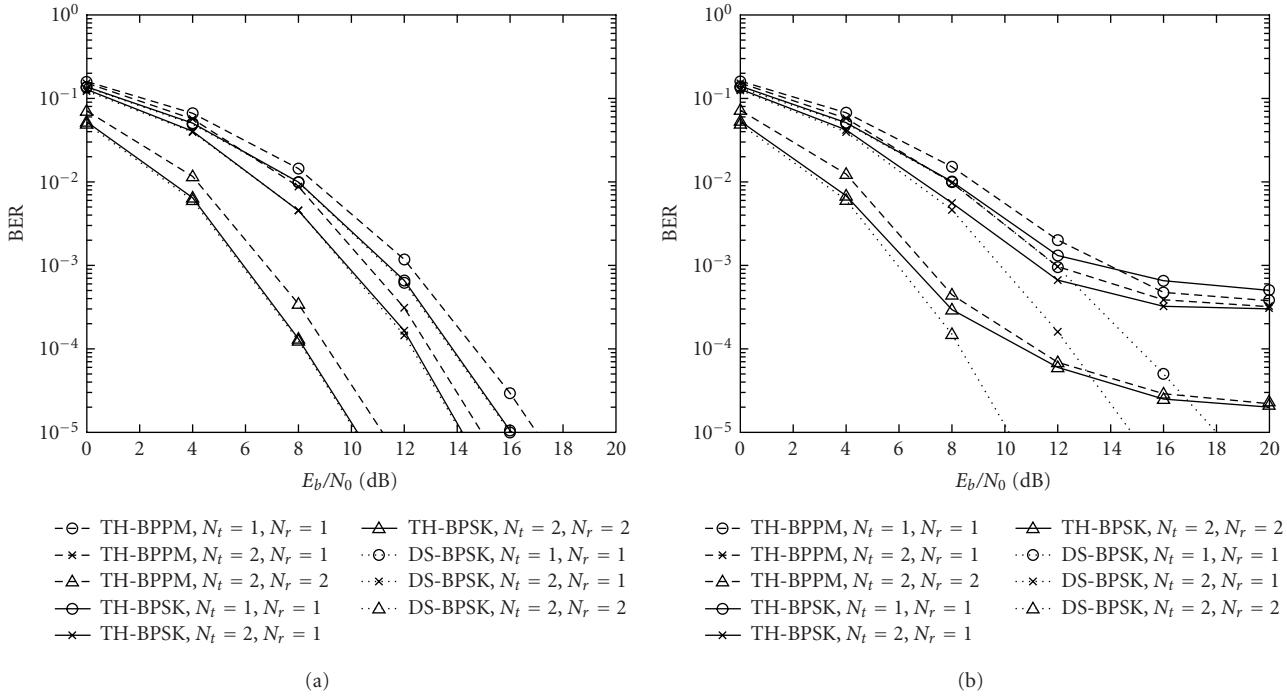

FIGURE 6: TH- and DS-UWB systems: (a) single user and (b) multiuser ($N_u = 5$).

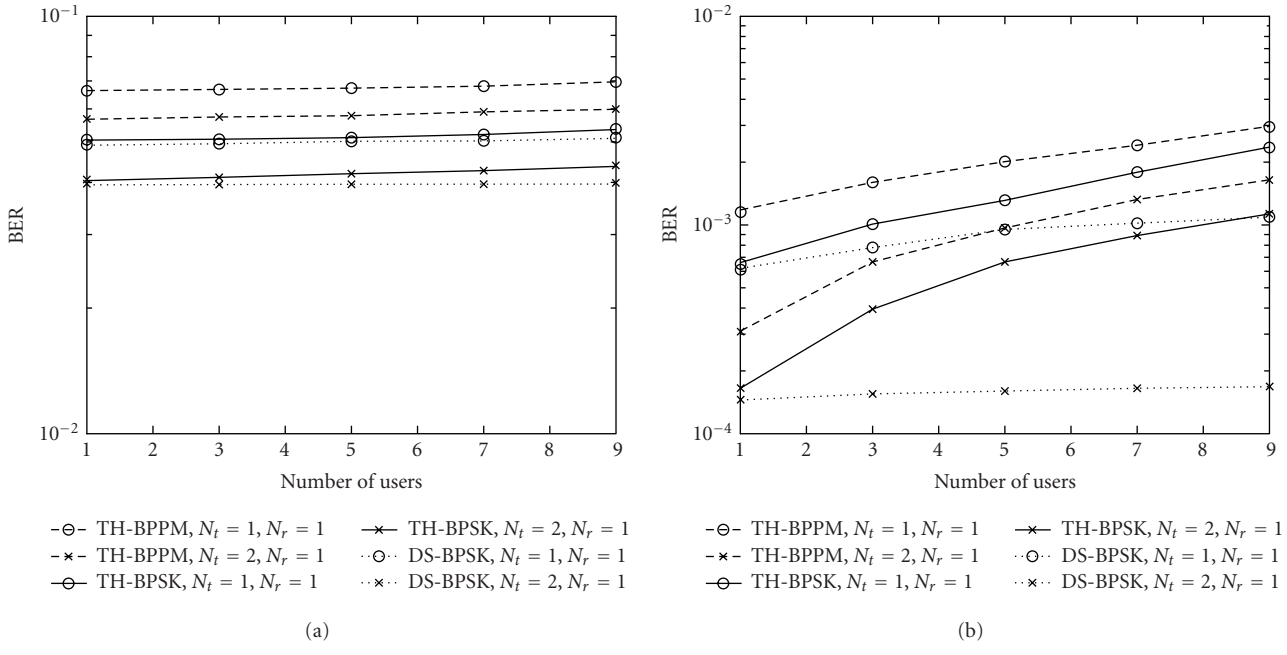

FIGURE 7: TH- and DS-UWB systems: (a) $E_b/N_0 = 4$ dB and (b) $E_b/N_0 = 12$ dB.

In Figures 7a and 7b, we plot the BER performances as a function of the number of active users with the fixed E_b/N_0 of 4 and 12 dB, respectively. In both cases, we observe performance degradation when more users are presented. For any number of users, the BPSK systems achieve better performance than the BPPM one. Comparing between TH and DS techniques, DS-BPSK performs slightly better than TH-BPSK at $E_b/N_0 = 4$ dB, and it remarkably outperforms TH-BPSK at $E_b/N_0 = 12$ dB, especially when the ROD-ST system is utilized. This is because with a fixed T_f and random

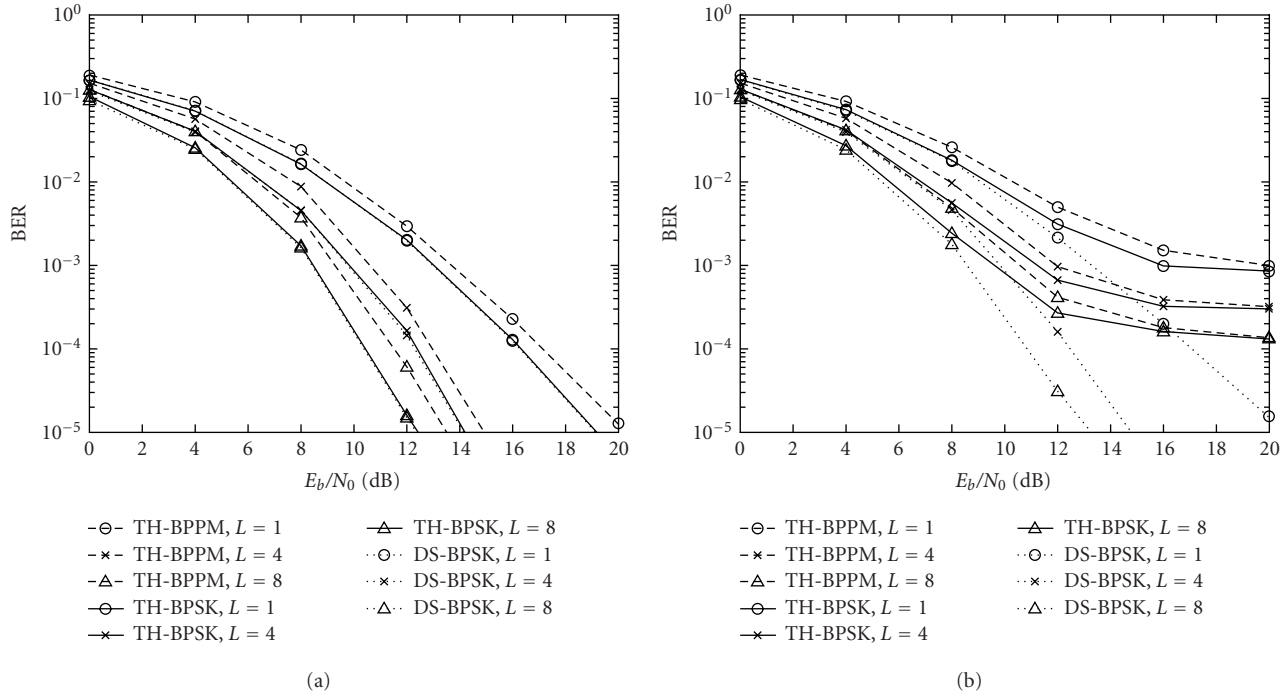

Figure 8: TH- and DS-UWB-MIMO systems with various L: (a) single user and (b) multiuser ($N_u = 5$).

spreading sequence, the MA interference of DS systems is less than that of TH systems [14, 15]. As we can see from Figure 7b, when the number of users increases, the BER of the TH-ST system increases much faster than that of the DS-ST system. Therefore, we can conclude that the DS-ST system is capable of accommodating multiple users with lower BER than TH systems.

Figures 8a and 8b demonstrate the effect of RAKE fingers to the performances of TH and DS schemes. Here, we consider UWB-ST systems with two transmit and one receive antennas. The BER versus E_b/N_0 curves for single-user and multiuser systems, each employing RAKE receivers with $L = 1$, 4, and 8 fingers, are shown in Figures 8a and 8b, respectively. The performance improvement with the increasing number of fingers can be observed from both figures. This corresponds to the fact that a RAKE receiver with more number of fingers provides higher capability to capture the available signal energy in dense multipath environments. Such improvement can be obviously seen in the single-user case. This supports our analytical results in the previous sections that the diversity gain is increasing with L. Nevertheless, in the presence of MAI, the performance improvement of TH systems degrades rapidly, as shown in Figure 8b. On the contrary, the benefit of additional fingers is evident for DS-BPSK system in both single-user and multiuser scenarios.

In Figures 9a and 9b, we show the performance of single- and multiuser systems employing ROD-ST codes with full and half rates. Both figures illustrate that utilizing either full- or reduced-rate code, BPSK provides lower BER than the BPPM scheme. From Figure 9a, we can see that the performances of full- and half-rate ROD codes are close to each other for every modulation schemes. This is in agreement with the results (78) and (80) in Section 5, which say that for a single-user system, decreasing the rate of the ROD-ST code does not improve the performance. Unlike the single-user case, the results in Figure 9b confirm our expectation, that when the code rate is lower, both TH-BPSK and TH-BPPM multiuser systems achieve better performances, especially in high-SNR regime. However, for DS-BPSK MA systems, the BER improvement obtained from reducing the code rate is insignificant. This is because for DS multiuser system with $N_u = 5$, the effect of MAI is considerably small, and ROD-ST code provides close to maximum achievable performance without decreasing the code rate. Once again, DS-BPSK outperforms other modulation schemes, for both full and half rates.

7. CONCLUSIONS

In this paper, we provide performance analysis for multi-antenna single-carrier UWB communication systems with various transmission schemes, including TH-BPPM, TH-BPSK, and DS-BPSK. Based on Nakagami-m frequency selective-fading channels, the performance metrics (diversity and coding gains) of UWB ST systems are quantified regardless of the particular coding scheme. We show that the use of ST coding in combination with RAKE architecture is able to exploit spatial diversity as well as multipath diversity,

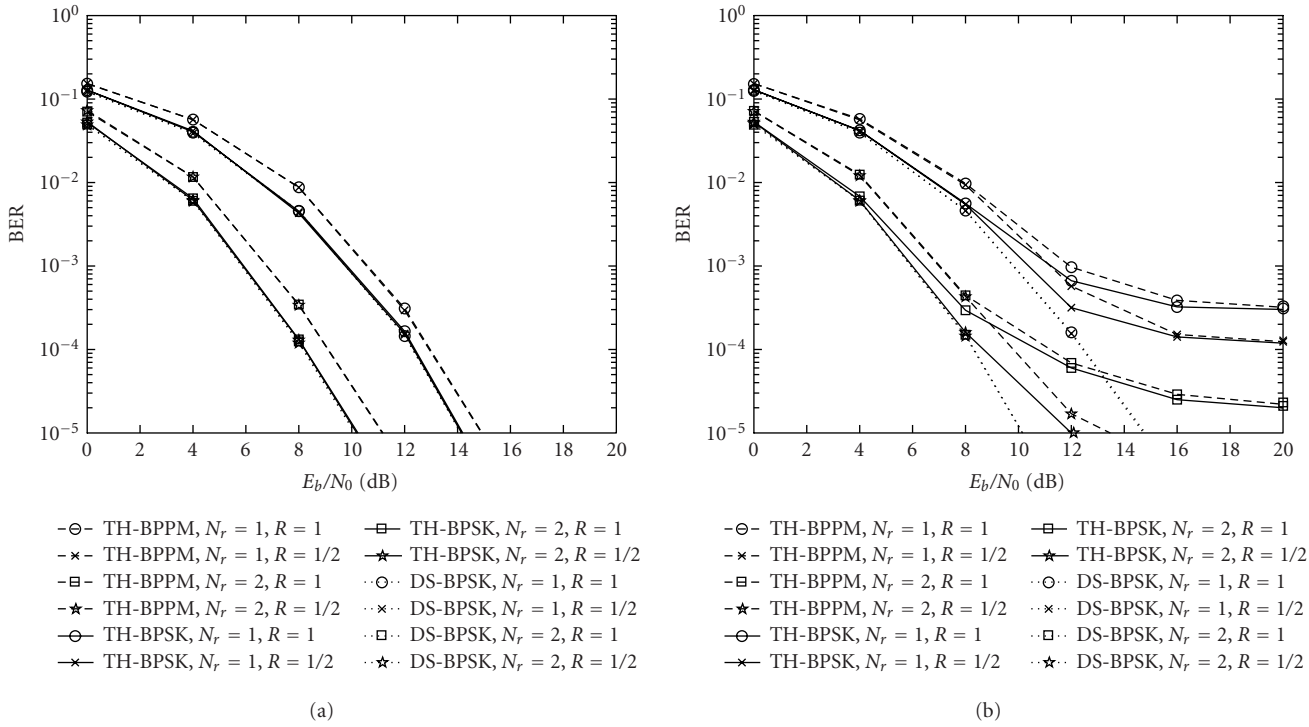

Figure 9: TH- and DS-UWB-MIMO systems with ROD-ST codes of different rates: (a) single user and (b) multiuser ($N_u = 5$).

inherent in UWB environments. An example of UWB ST signals based on the ROD-ST code for two-transmit-antenna systems is considered. Comparing various modulation techniques, we show that in the single-user case, the improvement of performances by using MIMO transmission is more significant in the case of TH-BPSK and DS-BPSK compared to that of TH-BPPM, whereas in MA scenarios, DS-BPSK outperform other schemes. For example, by employing two transmit and one receive antennas for a system of 5 users and $E_b/N_0 = 8$ dB, the BER for TH-BPPM decreases from 1.5×10^{-2} to 9.7×10^{-3}, for TH-BPSK from 10^{-2} to 5.6×10^{-3}, and for DS-BPSK from 10^{-2} to 4.6×10^{-3}. In addition, we show that reducing the rate of the UWB-ST code would not improve the performance of single-user systems for all modulation schemes. However, in multiuser environments, reducing the code rate improves the performances of TH systems, while the improvement in the DS system is not significant.

APPENDIX

EVALUATION OF $n^j_{p,k'}(l')$ IN (17)

We first express $n^j_{p,k'}(l')$ in (17) as

$$n^j_{p,k'}(l') = \sqrt{\frac{E_0}{N_t}} \sum_{i=0}^{N_t-1} n^{ij}_{p,k'}(l'), \tag{A.1}$$

where

$$n^{ij}_{p,k'}(l') \triangleq \sum_{l=0,l\neq l'}^{L_0-1} \alpha^{ij}_0(l) \left\{ \gamma\left[\tau_0(l)-\tau_0(l')+\frac{1-d^i_0(k')}{2}T_d\right] - \gamma\left[\tau_0(l)-\tau_0(l')+\frac{1-d^i_0(k')}{2}T_d-T_d\right]\right\}. \tag{A.2}$$

Recall from the definition of $\gamma(\cdot)$ in (11) that $\gamma[\tau_0(l)-\tau_0(l')+(1-d^i_0(k'))T_d/2]$ is nonzero only for $|\tau_0(l)-\tau_0(l')+(1-d^i_0(k'))T_d/2| < T_w$, that is,

$$\tau_0(l') - T_w - \frac{1-d^i_0(k')}{2}T_d < \tau_0(l) < \tau_0(l') + T_w - \frac{1-d^i_0(k')}{2}T_d. \tag{A.3}$$

Since we assume that $T_d < T_w$ and $\tau_0(l)-\tau_0(l-1) \geq T_w$, only $\tau_0(l) \in \{\tau_0(l'-1), \tau_0(l')\}$ satisfy (A.3). Similarly, $\gamma[\tau_0(l) - \tau_0(l') + (1-d^i_0(k'))T_d/2 - T_d]$ is nonzero for

$$\tau_0(l') - T_w - \frac{1-d^i_0(k')}{2}T_d + T_d < \tau_0(l) < \tau_0(l') + T_w - \frac{1-d^i_0(k')}{2}T_d + T_d \tag{A.4}$$

and only $\tau_0(l) \in \{\tau_0(l'), \tau_0(l'+1)\}$ satisfies (A.4). Therefore we can simplify the expression for $n^{ij}_{p,k'}(l')$ to

$$n^{ij}_{p,k'}(l') = \alpha^{ij}_0(l'-1)r^i_{k'}(l'-1) - \alpha^{ij}_0(l'+1)r^i_{k'}(l'+1), \quad (A.5)$$

where

$$\begin{aligned} r^i_{k'}(l'-1) &\triangleq \gamma\left[\tau_0(l'-1) - \tau_0(l') + \left(1 - d^i_0(k')\right)\frac{T_d}{2}\right] \\ &= \begin{cases} \gamma[\tau_0(l'-1) - \tau_0(l')] = 0, & d^i_0(k') = 1, \\ \gamma[\tau_0(l'-1) - \tau_0(l') + T_d], & d^i_0(k') = -1, \end{cases} \\ r^i_{k'}(l'+1) &\triangleq \gamma\left[\tau_0(l'+1) - \tau_0(l') + \left(1 - d^i_0(k')\right)\frac{T_d}{2} - T_d\right] \\ &= \begin{cases} \gamma[\tau_0(l'+1) - \tau_0(l') - T_d], & d^i_0(k') = 1, \\ \gamma[\tau_0(l'+1) - \tau_0(l')] = 0, & d^i_0(k') = -1. \end{cases} \end{aligned} \quad (A.6)$$

After some manipulations, we have

$$\begin{aligned} n^{ij}_{p,k'}(l') = {} & \alpha^{ij}_0(l'-1)\gamma[\tau_0(l') - \tau_0(l'-1) - T_d]\delta(d^i_0(k') + 1) \\ & - \alpha^{ij}_0(l'+1)\gamma[\tau_0(l'+1) - \tau_0(l') - T_d]\delta(d^i_0(k') - 1). \end{aligned} \quad (A.7)$$

We assume that the relative multipath gains follow the multipath intensity profile (MIP) model [26], which is defined such that the average power is one for the first path and $c\exp(-a\tau(l))s(\tau(l))$ for the path with relative delay $\tau(l)$. Here, c is a log-normal random variable, a is a Gaussian random variable with mean 0.19 (/ns) and variance 0.01, and $s(\tau)$ is a log-normal process over τ with fairly constant mean of 0.638. From the MIP model, the relationship between the gains of two consecutive paths can be written as

$$\alpha(l) = \frac{s(\tau(l))}{s(\tau(l-1))}\exp\left(-a\left(\tau(l) - \tau(l-1)\right)\right)\alpha(l-1). \quad (A.8)$$

Hence, (A.7) can be reexpressed as

$$\begin{aligned} n^{ij}_{p,k'}(l') = {} & \left\{ \frac{s(\tau(l'-1))}{s(\tau(l'))}\exp\left(-a\left(\tau(l'-1) - \tau(l')\right)\right)\right. \\ & \times\gamma[\tau_0(l') - \tau_0(l'-1) - T_d]\delta(d^i_0(k') + 1) \\ & - \frac{s(\tau(l'+1))}{s(\tau(l'))}\exp\left(-a\left(\tau(l'+1) - \tau(l')\right)\right) \\ & \times\gamma[\tau_0(l'+1) - \tau_0(l') - T_d] \\ & \left.\times\delta(d^i_0(k') - 1)\right\}\alpha^{ij}_0(l') \\ \triangleq {} & q^{ij}_{k'}(l')\alpha^{ij}_0(l'). \end{aligned} \quad (A.9)$$

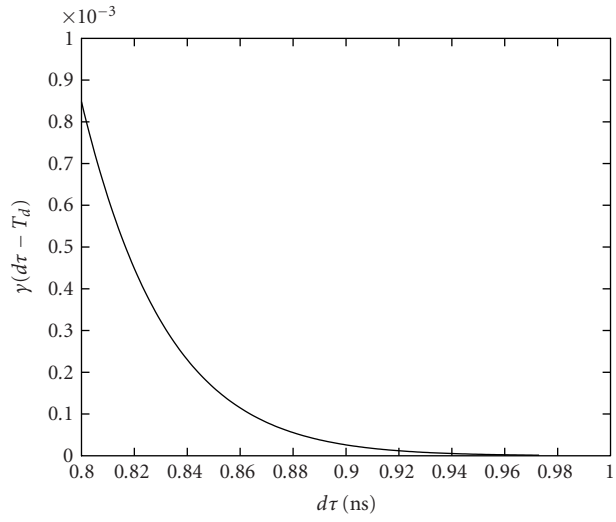

Figure 10: Correlation function $\gamma(d\tau - T_d)$ as a function of $d\tau$.

Recall from Section 3.1 that the correlator output corresponding to the desired user is

$$\begin{aligned} y^j_{d,k'}(l') &= \left[1 - \gamma(T_d)\right]\sqrt{\frac{E_0}{N_t}}\sum_{i=0}^{N_t-1} d^i_0(k')\alpha^{ij}_0(l') + n^j_{p,k'}(l') \\ &= \sqrt{\frac{E_0}{N_t}}\sum_{i=0}^{N_t-1}\left\{\left[1 - \gamma(T_d)\right]d^i_0(k')\alpha^{ij}_0(l') + n^{ij}_{p,k'}(l')\right\}. \end{aligned} \quad (A.10)$$

Substituting (A.9) into (A.10), we arrive at

$$y^j_{d,k'}(l') = \sqrt{\frac{E_0}{N_t}}\sum_{i=0}^{N_t-1}\left(\left[1 - \gamma(T_d)\right]d^i_0(k') + q^{ij}_{k'}(l')\right)\alpha^{ij}_0(l'). \quad (A.11)$$

Based on the parameters in Section 6 and the correlation function in (86), we display the correlation between the two monocycles whose delay difference is $d\tau - T_d$ in Figure 10. From Figure 10, we can see that $\gamma(d\tau - T_d) \le \gamma(T_w - T_d)$ for all $d\tau \ge T_w = 0.8$ nanosecond. Thus, $\gamma(\tau_0(l) - \tau_0(l-1) - T_d) \le \gamma(T_w - T_d)$ for any $l \in \{1, 2, \ldots, L_0 - 1\}$. Using (86) and the parameters in Section 6, the values of $\gamma(T_w - T_d)$ and $[1 - \gamma(T_d)]$ are found to be 8.48×10^{-4} and 1.618, respectively. Therefore, we can conclude that $n^j_{p,k'}(l')$ can be neglected without causing considerable effect to the performance evaluation.

REFERENCES

[1] Federal Communications Commission (FCC), "Revision of part 15 of the commission's rules regarding ultra-wideband transmission systems", First Report and Order, ET Docket 98–153, FCC 02-48, 02-48; Adopted: February 2002; Released: April 2002.

[2] J. R. Foerster, "Ultra-wideband technology for short-range, high-rate wireless communications," 2002, http://www.ieee.or.com/Archive.

[3] M. Z. Win and R. A. Scholtz, "Energy capture vs. correlator resources in ultra-wide bandwidth indoor wireless communications," in *Proc. IEEE Military Communications Conference (MILCOM '97)*, vol. 3, pp. 1277–1281, Monterey, Calif, USA, November 1997.

[4] S. M. Alamouti, "A simple transmit diversity technique for wireless communications," *IEEE J. Select. Areas Commun.*, vol. 16, no. 8, pp. 1451–1458, 1998.

[5] V. Tarokh, N. Seshadri, and A. R. Calderbank, "Space-time codes for high data rate wireless communication: Performance criterion and code construction," *IEEE Trans. Inform. Theory*, vol. 44, no. 2, pp. 744–765, 1998.

[6] V. Tarokh, H. Jafarkhani, and A. R. Calderbank, "Space-time block codes from orthogonal designs," *IEEE Trans. Inform. Theory*, vol. 45, no. 5, pp. 1456–1467, 1999.

[7] L. Yang and G. B. Giannakis, "Space-time coding for impulse radio," in *Proc. IEEE Conference on Ultra Wideband Systems and Technologies (UWBST '02)*, pp. 235–239, Baltimore, Md, USA, May 2002.

[8] N. A. Kumar and R. M. Buehrer, "Application of layered space-time processing to ultrawideband communication," in *Proc. 45th Midwest Symposium Circuits and Systems (MWSCAS '02)*, vol. 3, pp. 597–600, Tulsa, Okla, USA, August 2002.

[9] M. Weisenhorn and W. Hirt, "Performance of binary antipodal signaling over indoor UWB MIMO channel," in *Proc. IEEE International Conference on Communications (ICC '03)*, vol. 4, pp. 2872–2878, Anchorage, Alaska, USA, May 2003.

[10] W. Siriwongpairat, M. Olfat, and K. J. R. Liu, "On the performance evaluation of TH and DS UWB MIMO systems," in *Proc. IEEE Wireless Communications and Networking Conference (WCNC '04)*, vol. 3, pp. 1800–1805, Atlanta, Ga, USA, March 2004.

[11] R. A. Scholtz, "Multiple access with time-hopping impulse modulation," in *Proc. IEEE Military Communications Conference (MILCOM '93)*, vol. 2, pp. 447–450, Boston, Mass, USA, October 1993.

[12] M. L. Welborn, "System considerations for ultra-wideband wireless networks," in *Proc. IEEE Radio and Wireless Conference (RAWCON '01)*, vol. 2, pp. 5–8, Waltham, Mass, USA, August 2001.

[13] J. R. Foerster, "The performance of a direct-sequence spread ultrawideband system in the presence of multipath, narrowband interference, and multiuser interference," in *Proc. IEEE Conference on Ultra Wideband Systems and Technologies (UWBST '02)*, pp. 87–91, Baltimore, Md, USA, May 2002.

[14] N. Boubaker and K. B. Letaief, "Ultra wideband DSSS for multiple access communications using antipodal signaling," in *Proc. IEEE International Conference on Communications (ICC '03)*, vol. 3, pp. 2197–2201, Anchorage, Alaska, USA, May 2003.

[15] V. S. Somayazulu, "Multiple access performance in UWB systems using time hopping vs. direct sequence spreading," in *Proc. IEEE Wireless Communications and Networking Conference (WCNC '02)*, vol. 2, pp. 522–525, Orlando, Fla, USA, March 2002.

[16] G. Durisi and S. Benedetto, "Performance evaluation and comparison of different modulation schemes for UWB multiaccess systems," in *Proc. IEEE International Conference on Communications (ICC '03)*, vol. 3, pp. 2187–2191, Anchorage, Alaska, USA, May 2003.

[17] J. G. Proakis, *Digital Communications*, McGraw-Hill, New York, NY, USA, 4th edition, 2001.

[18] M. Z. Win and R. A. Scholtz, "Ultra-wide bandwidth time-hopping spread-spectrum impulse radio for wireless multiple-access communications," *IEEE Trans. Commun.*, vol. 48, no. 4, pp. 679–689, 2000.

[19] R. J. Cramer, M. Z. Win, and R. A. Scholtz, "Evaluation of the multipath characteristics of the impulse radio channel," in *Proc. 9th IEEE International Symposium on Personal, Indoor and Mobile Radio Communications (PIMRC '98)*, vol. 2, pp. 864–868, Boston, Mass, USA, September 1998.

[20] M. Z. Win and R. A. Scholtz, "Impulse radio: How it works," *IEEE Communications Letters*, vol. 2, no. 2, pp. 36–38, 1998.

[21] C. M. Canadeo, M. A. Temple, R. O. Baldwin, and R. A. Raines, "Code selection for enhancing UWB multiple access communication performance using TH-PPM and DS-BPSK modulations," in *Proc. IEEE Wireless Communications and Networking Conference (WCNC '03)*, vol. 1, pp. 678–682, New Orleans, La, USA, March 2003.

[22] M. Nakagami, "The *m*-distribution: A general formula of intensity distribution of rapid fading," in *Statistical Methods in Radio Wave Propagation*, W. G. Hoffman, Ed., pp. 3–36, Pergamon, Oxford, UK, 1960.

[23] R. A. Horn and C. R. Johnson, *Matrix Analysis*, Cambridge University Press, New York, NY, USA, 1985.

[24] M. K. Simon and M. S. Alouini, *Digital Communication over Fading Channels: A Unified Approach to Performance Analysis*, John Wiley & Sons, New York, NY, USA, 2000.

[25] F. Ramirez-Mireles and R. A. Scholtz, "Multiple-access performance limits with time hopping and pulse position modulation," in *Proc. IEEE Military Communications Conference (MILCOM '98)*, vol. 2, pp. 529–533, Boston, Mass, USA, October 1998.

[26] S. S. Ghassemzadeh, L. J. Greenstein, T. Sveinsson, and V. Tarokh, "A multipath intensity profile model for residential environments," in *Proc. IEEE Wireless Communications and Networking Conference (WCNC '03)*, vol. 1, pp. 150–155, New Orleans, La, USA, March 2003.

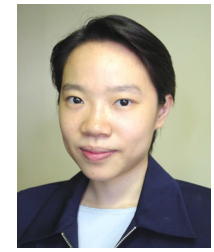

W. Pam Siriwongpairat received the B.S. degree in electrical engineering from the Chulalongkorn University, Bangkok, Thailand, in 1999, and the M.S. degree in electrical engineering from the University of Maryland, College Park, in 2001. She is currently a Ph.D. student in the Department of Electrical and Computer Engineering and Institute for Systems Research, the University of Maryland, College Park. Her current research interests include signal processing, wireless communications, and networking, with particular focus on ultra-wideband communications. Her research encompasses space-time and space-frequency coding for multiantenna ultra-wideband systems.

Masoud Olfat received the B.S. degree in electrical engineering from Sharif University of Technology, Tehran, Iran, in 1993, and the M.S. and Ph.D. degrees both in electrical engineering from the University of Maryland, College Park, in 1998 and 2003, respectively. From October 1995 to August 1996, he worked at CASE Center, Syracuse University, Syracuse, NY, as a Research Assistant. In 1998, he joined Odyssey Technology Inc., Laurel, Md, working as a member of the technical staff. He consulted for Hermes Technologies Inc., Athens, Greece, in 2001, on the development of IEEE 802.11a MAC product. He is currently a Senior Manager in Technology Evaluation and Research Department, Nextel Communications Inc., working on the evaluation and development of broadband wireless access technologies,

while holding a Postdoctoral Research Associate appointment with the Institute for Systems Research, the University of Maryland, College Park. His current research interests include statistical signal processing, coding, power control, multiple antenna schemes (including beamforming, spatial multiplexing, and space-time and frequency coding), scheduling, and QoS schemes for wireless communications systems, with a special interest in OFDM and UWB systems. Dr. Olfat ranked first in the Iranian universities' nationwide entrance examinations in the western provinces of Iran in 1984.

K. J. Ray Liu received the B.S. degree from the National Taiwan University in 1983, and the Ph.D. degree from UCLA in 1990, both in electrical engineering. He is a Professor in the Electrical and Computer Engineering Department and Institute for Systems Research, the University of Maryland, College Park. His research contributions encompass broad aspects of multimedia communications and signal processing; wireless communications and networking; information security; signal processing algorithms and architectures; and bioinformatics, in which he has published over 300 refereed papers. Dr. Liu is the recipient of numerous honors and awards including IEEE Signal Processing Society 2004 Distinguished Lecturer, the 1994 National Science Foundation Young Investigator Award, the IEEE Signal Processing Society's 1993 Senior Award (Best Paper Award), and the IEEE 50th Vehicular Technology Conference Best Paper Award, Amsterdam, 1999. He also received the George Corcoran Award in 1994 for outstanding contributions to electrical engineering education and the Outstanding Systems Engineering Faculty Award in 1996 in recognition of outstanding contributions in interdisciplinary research, both from the University of Maryland. Dr. Liu is a Fellow of IEEE. Dr. Liu is the Editor-in-Chief of IEEE Signal Processing Magazine and was the Founding Editor-in-Chief of EURASIP Journal on Applied Signal Processing. Dr. Liu is a Board of Governor and has served as a Chairman of the Multimedia Signal Processing Technical Committee of IEEE Signal Processing Society.

EURASIP JOURNAL ON ADVANCES IN SIGNAL PROCESSING

Special Issue on
3DTV: Capture, Transmission and Display of 3D Video

Call for Papers

Capturing three-dimensional visual information of a real-life scene and creating an exact (except the scale) optical duplicate of it at a remote site instantaneously, or at a later time, are ultimate goals in visual communications. All core and peripheral components related to this goal are collectively referred to as "three-dimensional television (3DTV)." Main functional components of 3DTV are "capture and representation of 3D scene information," "complete definition of digital 3DTV signal," "storage and transmission of this signal," and finally the "display of the reproduced 3D scene." For a successful consumer accepted operation of 3DTV, all these functional components must be carefully designed in an integrated fashion by considering the harmonious interaction among them. This kind of large-scale integration naturally involves a large group of researchers with diverse backgrounds, and therefore has a highly multidisciplinary nature.

The objective of the proposed special issue is to present, in a well-coordinated fashion, the works and efforts of researchers with rather diverse experience and activity in distinct, yet related and complementary areas for achieving full-scale three-dimensional television. The latest research contributors in the field and authors of selected papers of the 3DTV CON 2007 (www.3dtv-con.org) will be invited to this special issue.

Papers on the following and related list of topics are solicited:

- 3D Capture and processing
  - 3D time-varying scene capture technology
  - Multicamera recording
  - 3D photography algorithms
  - Synchronization and calibration of camera arrays
  - 3D view registration
  - Multiview geometry and calibration
  - Holographic camera techniques
  - 3D motion analysis and tracking
  - Surface modeling for 3D scenes
  - Multiview image and 3D data processing
- 3D transmission
  - Systems, architecture, and transmission aspects of 3D
  - 3D streaming
  - Error-related issues and handling of 3D video
  - Hologram compression
  - Multiview video coding
  - 3D mesh compression
  - Multiple-description coding for 3D
  - Signal processing for diffraction and holographic 3DTV
- 3D visualization
  - 3D mesh representation
  - Texture and point representation
  - Object-based representation and segmentation
  - Volume representation
  - 3D motion animation
  - Dense stereo and 3D reconstruction
  - Stereoscopic display techniques
  - Holographic display technology
  - Reduced parallax systems and integral imaging
  - Underlying optics and VLSI technology
  - Projection and display technology for 3D videos
  - Human factors
- 3D applications
  - 3D imaging in virtual heritage and virtual archaeology
  - 3D teleimmersion and remote collaboration
  - Augmented reality and virtual environments
  - 3D television, cinema, games, and entertainment
  - Medical and biomedical applications
  - 3D content-based retrieval and recognition
  - 3D watermarking

Authors should follow the EURASIP Journal on Advances in Signal Processing manuscript format described at the journal site http://www.hindawi.com/journals/asp/. Prospective authors should submit an electronic copy of their complete manuscript through the EURASIP Journal on Advances in Signal Processing Manuscript Tracking Sys-

tem at http://mts.hindawi.com/, according to the following timetable:

Manuscript Due	October 1, 2007
First Round of Reviews	January 1, 2008
Publication Date	April 1, 2008

Guest Editors:

Levent Onural, Department of Electrical and Electronics Engineering, Bilkent University, 06800 Bilkent, Ankara, Turkey; onural@ee.bilkent.edu.tr

Aljoscha Smolic, Fraunhofer-Institut für Nachrichtentechnik Heinrich-Hertz-Institut, 10587 Berlin, Germany; smolic@hhi.de

A. Enis Cetin, Department of Electrical and Electronics Engineering, Bilkent University, 06800 Bilkent, Ankara, Turkey; cetin@ee.bilkent.edu.tr

John Watson, Department of Engineering, University of Aberdeen, Scotland AB24 3UE, UK; j.watson@abdn.ac.uk

Georgios A. Triantafyllidis, Informatics and Telematics Institute, Center for Research and Technology-Hellas/CERTH, 57001 Thermi-Thessaloniki, Greece; gatrian@iti.gr

Thomas Sikora, Institut für Telekommunikationssysteme, Technische Universität Berlin, 10587 Berlin, Germany; sikora@nue.tu-berlin.de

Third International Conference on Image and Signal Processing

ICISP 2008

July 1-3, Cherbourg-Octeville, Normandy, France

CALL FOR PAPERS

Following the two successful previous editions of ICISP (Agadir 2001, Agadir 2003), the *Université de Caen Basse Normandie* will organize the next ICISP event in Cherbourg-Octeville, Normandy, France. ICISP aims to provide researchers and practitioners from academia and industry with a forum on the last developments in image and signal processing, multimedia and computer graphics. The conference will also provide a unique opportunity for sharing experiences from different backgrounds with the common interest in advanced methods in the above-mentioned fields. The scientific program of ICISP 2008 will include the presentation of invited plenary talks, special sessions as well as poster and regular sessions with contributed research papers.

Topics of interest for submission include, but are not limited to:

- Image and video processing: image filtering, restoration and enhancement, image segmentation, video segmentation and tracking, morphological processing, feature extraction and analysis, interpolation and super-resolution, motion detection and estimation, computer vision, pattern recognition, content-based image retrieval.
- Signal Processing: spectral analysis, time-frequency and time-scale representation, statistical signal processing, filtering, detection and estimation, nonlinear signal processing, radar, antennas, telecommunications systems, acoustics.
- Computer graphics: algorithms, visualization, animation, virtual reality.
- Applications: biomedical sciences, biometry, document image processing and authentication, other applications.

ICISP 2008 will also include a number of special sessions :

- Image mass data analysis,
- Graph-based representations in pattern recognition,
- Biomedical applications: Virtual slide acquisition and processing.

PAPER SUBMISSION

Prospective authors are invited to submit full papers of not more than eight (8) pages including results, figures and references. All the papers will be handled and reviewed electronically through the conference web site.

Submission of full paper	**January 25, 2008**
Notification of acceptance	**March 10, 2008**
Submissions of camera-ready papers	**April 10, 2008**

CONFERENCE VENUE

ICISP'2008 will be held in Cherbourg-Octeville (France) on July 1-3, 2008.

For further information: http://www.stlo.unicaen.fr/icisp2008